Supporting Information

Nano-Optical Biomolecular Interaction Sensing within Complex Media via Peptide Hybrid Ligand Conjugation

Gurunath Apte,[1,2] † Moritz Roman Schepp,[1,2] † Haydn L. Ball,[3,4] Niklas Halbwedl,[5] Peijian Zou,[6,7] Na Sun,[8] Axel Walch,[8] Martin Zacharias,[5] Michael Sattler,[6,7] Oliver Plettenburg,[3,4] Jian Cui[1,2,9]*

[1]Helmholtz Pioneer Campus, Helmholtz Munich, Neuherberg, Germany
[2]Photonic Biosystems and Technologies, Bioengineering Center, Helmholtz Munich, Neuherberg, Germany
[3]Institute of Medicinal Chemistry, Molecular Targets and Therapeutics Center, Helmholtz Munich, Neuherberg, Germany
[4]Institute of Organic Chemistry, Leibniz University Hannover, Hannover, Germany
[5]Department of Bioscience, TUM School of Natural Sciences, Physics Department and Center of Protein Assemblies, Technical University of Munich, Garching, Germany
[6]Institute of Structural Biology, Molecular Targets and Therapeutics Center, Helmholtz Munich, Neuherberg, Germany
[7]Bavarian NMR Center, Department of Bioscience, TUM School of Natural Sciences, Technical University of Munich, Garching, Germany
[8]Research Unit Analytical Pathology, Helmholtz Munich, Neuherberg, Germany
[9]Department of Bioscience, TUM School of Natural Sciences, Technical University of Munich, Garching, Germany

† These authors contributed equally
*Corresponding Author

MATERIALS & METHODS

Nanoparticle Synthesis

Silver decahedral nanoparticles (AgDNP) were synthesized by generally following the same method we used previously.[1] A home-built photoreactor equipped with 445 nm LEDs was used. (Intelligent LED Solutions, ILH-ON09-DEBL-SC211-WIR200). Milli-Q water (14 mL), sodium citrate tribasic dihydrate (0.52 mL, 50 mM) (BioUltra, 71402), poly(sodium 4-styrenesulfonate) (0.023 mL, 2 mg/mL) (average Mw ~70 kDa, Sigma-Aldrich, 243051), L-arginine (Thermo Scientific Chemicals (0.025 mL, 5 mM), A15738.36), silver nitrate (0.4 mL, 5 mM) (Sigma-Aldrich, 209139), and freshly prepared sodium borohydride (0.2 mL, 0.1 M) (Sigma-Aldrich, 213462) were added to a 20 mL glass scintillation vial. This solution was stored for 50 min in the dark (nucleation phase), after which the solution changed its color from pale yellow to bright yellow. Then, hydrogen peroxide (0.3 mL, 30%) (VWR, AnalaR NORMAPUR, 23615.261) was added, followed by vigorous vortexing for 10 s. The vial was then immediately positioned 10 mm above the LED of the photoreactor and illuminated for 7 hours (**Figure S2**). The LED was turned on beforehand to stabilize intensity, and the intensity was set to 120 mW/cm^2 (measured directly above the LED) before sample exposure.

Gold Coating of Silver Decahedral Nanoparticles (AgDNP@Aus).

Gold coating of silver decahedral nanoparticles (AgDNPs) was performed according to a previously reported procedure.[1] Briefly, aqueous $HAuCl_4$ solution (3 mL, 0.0128 mM) (Sigma-Aldrich, 520918) was added dropwise (0.25 mL/h) over 12 h to the AgDNP solution (3 mL) under constant stirring at 500 rpm at room temperature in the dark.

Nanoparticle Characterization (UV–vis, DLS, zeta potential).

UV–vis extinction spectra were recorded using a Jasco V-760 spectrophotometer. The hydrodynamic diameter (by dynamic light scattering) and zeta potential of the nanoparticles were measured with a Malvern Zetasizer Ultra. For these measurements, nanoparticles were resuspended in 1 mM NaCl in H_2O (conductivity ≈ 250 $\mu S \cdot cm^{-1}$), and zeta potential measurements were performed with an applied voltage of 150 V.

Synthesis of Antifouling CysPoly(AEEA) Ligands / PEG–Peptide Hybrids.

Fmoc-amino acids, Fmoc-amino-3,5-dioxaoctanoic acid, and Fmoc-azidoalanine were purchased from either Novabiochem or Fluorochem. Protide amide resin was purchased from CEM. LPETGGG-Am peptides were synthesized on the microwave-assisted CEM peptide synthesizer (Matthews, NC, USA). All other couplings were performed manually using a 4-fold excess of carboxylic acid reagent and acylations using 2-(7-Aza-1H-benzotriazole-1-yl)-1,1,3,3-tetramethyluronium hexafluorophosphate (HATU)/Diisopropylethylamine (DIEA) activation. The final acetylation of the N-terminus was achieved using 10% Acetic anhydride and 5% DIEA in N-Methylpyrrolidone (NMP).

Final cleavage was achieved using 95% Trifluoroacetic acid (TFA) containing 2,2-(Ethylenedioxy)diethanethiol and Triisopropylsilane (2:1) scavengers. The cleavage reaction was performed at room temperature for 1.5 h. The cleaved crude peptide was precipitated in cold diethyl ether, centrifuged and washed several times with fresh cold ether. If the crude peptide dissolved in ether it was rotary evaporated until dry and residue dissolved in water.

Crude peptides were purified on a Macherey-Nagel C18 semi-preparative reversed-phase HPLC column (250x10mm) using a Knauer 2.1 HPLC system. Fractions were analyzed on a Waters LCT LCMS and Phenomenex C18 analytical column (50 x 2.1 mm). Separations were achieved using linear gradients of 0–100% buffer B for 1 h (semipreparative) or 5 min (analytical), at a flow rate of 3 mL/min or 0.6 mL/min, respectively. Buffer A was water containing 0.05% TFA and buffer B was acetonitrile with 0.05% TFA. For the LCMS analysis, the buffers were the same as for the semi-preparative chromatography except with 0.1% Formic acid as a counterion. The best fractions were combined and lyophilized.

Table S1. List of CysPoly(AEEA) ligands used. Ligands modified exclusively with a terminal azide (Entry 2) or an "LPETGGG" motif (Entry 3) were used for strain-promoted azide–alkyne cycloaddition (SPAAC) and sortase-mediated ligation (SML), respectively. CysPoly(AEEA) without conjugation moieties was used for backfilling to enhance nanobiosensor stability and antifouling. -am refers to C-terminal amidation.

Entry	**Name**	**Sequence**	**MW (Da)**	**Use**
1	CysPoly(AEEA)	Ac-Cys-$(AEEA)_4$-am	742.5	Backfilling
2	CysPoly(AEEA) azido-alanine	Ac-Cys-$(AEEA)_7$-Aza-am	1292.4	SPAAC
3	CysPoly(AEEA) LPETGGG	Ac-Cys-$(AEEA)_5$-LPETGGG-am	1500.9	SML

Protein Production / Synthesis.

The protein constructs of the N-terminal disordered region of the peroxisomal receptor PEX5 (residues 1–113, referred to as "PEX51"), PEX5 (residues 110–230, referred to as "PEX52"), and the N-terminal globular domain of peroxisomal PEX14 (residues 16–80) were sourced from previous studies.[2,3] These genes were cloned into two distinct vectors. Specifically, they were cloned into the pETM10 vector, which features a non-cleavable N - terminal His_6- tag, and the pETM11 vector, which has a His_6-tag followed by a tobacco etch virus (TEV) cleavage site (obtained from EMBL, G. Stier). The cloning process utilized the NcoI and KpnI restriction sites.

PEX52 was expressed using the pETM10 vector, leading to the production of a protein with a non-cleavable N-terminal His_6-tag, named His-PEX52. Meanwhile, PEX51, PEX52, and PEX14 were expressed on the pETM11 vector. After expression, the N-terminal His_6-tag was removed by TEV proteinase, resulting in the proteins named PEX51, PEX52, and PEX14 respectively.

PEX52 and PEX14 variants were generated by mutating the last amino acid, glycine, at the TEV cleavage site (ENLYFQG) to cysteine or serine in the pETM11-PEX52 and pETM11-PEX14 constructs. As a result, after TEV cleavage, these proteins had cysteine or serine as the first amino acid at their N - termini respectively. Mutations were carried out according to the strategy described in Beyer et al.[4]

The gene of the Sortase A (21-207) tetra mutant (P94S, D160N, D165A, K196T) was optimized based on the codon usage of Escherichia coli (E. coli) and directly ordered from Integrated DNA Technologies (IDT, Europe). This gene was cloned into the pETMGb1 vector, which has an N-terminal His_6-tag and a GB1 fusion protein followed by a TEV cleavage site. Additionally, the glycine at the TEV cleavage site was mutated to serine.

The constructed vectors were transformed into E. coli BL21 (DE3) cells and expressed in lysogeny broth (LB) medium. The protein samples were prepared following the protocol described in Zhou et al.[1] All proteins were initially purified using gravity - flow Ni - NTA affinity chromatography (Qiagen) with imidazole (300 mM). For non - His-tagged proteins, after TEV cleavage, they were further purified using a reverse Ni^{2+} column. Subsequently, all proteins were purified by size-exclusion chromatography (Superdex S75, 16/600, GE) in a buffer composed of HEPES (25 mM) (pH 7.5), NaCl (150 mM), and TCEP(1 mM).

The Sortase tetra mutant (SOR4M) was prepared as described by Freiburger et al. in 2015.[5] The final samples obtained from the size-exclusion chromatography were collected, concentrated, and then transferred to a buffer containing HEPES (25 mM) (pH 7.5), NaCl (150 mM), and 1 mM TCEP (1 mM). The His-SOR4M was the fusion protein without undergoing TEV cleavage.

Ligand and Protein Bioconjugation

Sortase-mediated ligation

A 120 μL ligation reaction containing CysPoly(AEEA)-LPETGGG (100 μM), PEX51 (100 μM), and His-tagged sortase-4M (10 μM) in ligation buffer (10 mM Tris-HCl, 50 mM NaCl, pH 7.5) was incubated on ice at 4 °C for 3 h with gentle shaking. The enzyme was removed by adding Ni-NTA magnetic agarose beads (100 μL, 5%) with a binding capacity of > 75 mg/ml (SERVA, 42179.02). After gentle mixing using a shaker for 30 min on ice, the beads were separated using a magnet, and the supernatant was collected. The ligation product was desalted using a Zeba Spin Desalting Column (7 kDa MWCO, Thermo Fisher, 89882) to remove cleaved triglycine byproducts and any unligated CysPoly(AEEA)-LPETGGG. The purified ligation product was then grafted onto the nanoparticles (see below).

Protein Maleimide-DBCO modification

Proteins with a surface-accessible C-terminal cysteine were labeled with DBCO-maleimide via thiol–maleimide coupling. Before labeling, the protein of interest (POI) was buffer-exchanged into N_2-degassed PBS (pH 6.5–7.5) using Zeba 7 kDa MWCO spin columns (Thermo Scientific 89877), adjusting sample volumes to 60–100 μL for optimal desalting. To reduce unwanted disulfide formation, TCEP (Sigma-Aldrich 646547) was added at a 2–5× molar excess and incubated for 20 min at room temperature. DBCO-PEG_4-maleimide (10 mM in DMSO, Sigma-Aldrich 760676) was then added at ≤20% of the reaction volume, using a POI:DBCO ratio of ~1:2. Reactions were performed in low-binding, light-protected tubes for up to 2 h on ice with mild shaking (200 rpm). Excess reagent was removed by buffer exchange using Zeba 7 kDa MWCO spin columns (Thermo Scientific 89877). When the extinction coefficient of POI at 280 nm (ε_{280}) was of the same order of magnitude as that of DBCO at 309 nm (ε_{309}), conjugation efficiency was determined by UV–vis spectroscopy. The degree of labeling (DOL) was calculated from absorbance values at 280 nm (A_{280}) and 309 nm (A_{309}), using reported extinction coefficients (ε_{309} = 12,000 M^{-1} cm^{-1}) and applying a correction factor of 1.089 to account for DBCO absorbance at 280 nm.

Strain-Promoted Azide–Alkyne Cycloaddition (SPAAC) Between POI–DBCO and CysPoly(AEEA)-Aza-Amide

SPAAC reactions were carried out by adding azide-functionalized peptide (CysPoly(AEEA)-Aza-Amide) dissolved in Milli-Q water to DBCO-labeled protein (POI–DBCO) at a 2–4× molar excess. As a reference, a 2× excess corresponds to adding 44 μL of 2 mM CysPoly(AEEA)-Aza-Amide to 110 μL of approximately 400 μM POI–DBCO. Reactions were incubated overnight at 4 °C in the dark. Unreacted peptide was removed by buffer exchange into a protein-stabilizing buffer of choice using Zeba 7 kDa MWCO spin columns or Amicon Ultra centrifugal concentrators. Purified conjugates were further stabilized with 0.025% Tween-20 and stored at 4 °C for up to one week.

Functionalization of AgDNP@Au Nanoparticles With POI–CysPoly(AEEA) Conjugates (via SPAAC or SML)

AgDNP@Au nanoparticles were functionalized with thiolated POI–peptide conjugates (POI–CysPoly(AEEA)). About 1.4 mL of AgDNP@Au colloids in native solution (Abs ~ 1.0) was centrifuged at 2,504 × g for 30 min, the supernatant removed, and the pellet resuspended in Milli-Q water (0.5 mL). The suspension was diluted to an extinction of ~1.4, and 289 µL was transferred to Protein LoBind tubes. Samples were centrifuged at 10,870 × g for 8–10 min, the supernatant removed, and pellets mixed with 5–15 µL of purified POI–CysPoly(AEEA). Pellets were resuspended in Tween-containing buffer (e.g., 10 mM Tris, 50 mM NaCl, 0.025% Tween-20), yielding ~10 µM POI–CysPoly(AEEA) and ~0.1 nM nanoparticles (~16× ligand excess to estimated surface binding sites). When needed, premixed ligand solutions (e.g., CysPoly(AEEA):POI–CysPoly(AEEA)) were prepared before nanoparticle coupling. Reactions were incubated for 2 h on ice, 1 h at room temperature, or overnight at 4 °C. For back-filling, excess CysPoly(AEEA) (e.g., 15 µL of 2 mM) was added after the initial 1 h and incubated for 1 h. Functionalized nanoparticles were collected by centrifugation at 10,867 × g (or 5,400 × g) for 8–10 min at 4 °C, washed twice with a buffer (**SI Table 2**) , and used directly for downstream binding experiments.

Nanobiosensor Characterization (sortase substrate assay, MALDI).

Sortase substrate assay

Reactions were set up in black 96-well plates containing Tris-HCl (10 mM), NaCl (50 mM), Tween-20 (0.025%), pH 7.5. The Bacterial Sortase Substrate III, Abz/DNP peptide(Anaspec, AS-63717) was mixed with a protein carrying an N-terminal glycine, and the reaction was initiated with sortase. Cleavage was monitored by fluorescence (λ_{ex} = 320 nm, λ_{em} = 420 nm) at room temperature using a Berthold Mithras² Plate Reader (LB943). The samples were stored at 4 °C between the measurement time points.

MALDI-TOF

One microliter of each sample was mixed with 1 µL of matrix solution containing sinapinic acid (10 mg/mL) dissolved in 60% acetonitrile and 0.2% (v/v) trifluoroacetic acid (REF 400003, Applied Biosystems). Samples were analyzed using a Bruker Ultraflex III MALDI-TOF/TOF mass spectrometer equipped with a SmartBeam laser. Spectra were acquired in linear positive-ion mode over a mass range of 4,000–29,500 Da with a sampling rate of 0.1 GS/s. Each spectrum represented the accumulation of 200 laser shots per pixel at constant laser power. External calibration was performed using Protein Calibration Standard I (Bruker Daltonics GmbH) spotted on the same target plate. Data were processed using FlexAnalysis software (version 3.4, Bruker Daltonics GmbH), including smoothing, normalization, baseline subtraction, and automatic peak picking.

LC-MS characterization of CysPoly(AEEA) ligands

Samples were dissolved in water and 10µl was loaded on the ThermoFisher LCMS consisting of a Dionex Ultimate 3000 UHPLC and a Thermo Scientific ISQ-EC operating in positive mode. A gradient of 0% water to 100% acetonitrile in 30 mins at a flow rate of 0.3ml/min was applied to elute the peptides on a Machery-Nagel EC50/2 Nucleodur C18 Pyramid RP-HPLC capillary column. Peaks were detected at 220nm.

Protein-Protein Interaction Sensing in Buffer, FBS and Human Serum (binding curve, K_D, BSA controls, kinetic).

NPs grafted with the peptide–protein complex were centrifuged twice at 5,400 rcf, and the resulting pellet was collected. The pellet was gently redispersed either in buffer or FBS, depending on the experiment (**Table S2**). Prior to sample measurements, baseline spectra were recorded using the corresponding blank (buffer or FBS). UV–vis spectra of the redispersed NPs were then acquired under identical instrumental settings.

For measurements performed in FBS, samples were allowed to equilibrate for 30 min after redispersion to ensure spectral stabilization. A concentration-dependent titration was subsequently carried out by sequentially adding small, defined aliquots of the second protein construct (PEX14). After each addition, samples were gently mixed on an orbital shaker for 2–3 min, followed by acquisition of the UV–vis spectrum. Cumulative PEX14 concentrations were calculated while accounting for dilution at each titration step. All protein stock solutions and intermediate dilutions were maintained on ice throughout the experiment.

For analyte quantification in human serum, nanoparticle pellets were redispersed in 800 µL of 25% (v/v) human serum (Sigma Aldrich, H3422) and incubated for 30 min to reach equilibrium. A concentration-dependent titration was then performed, as described above, to construct the standard calibration curve. For sample quantification, NP pellets were redispersed in triplicate in 800 µL of 25% human serum (Sigma Aldrich, H3422) containing the target analyte, incubated for 30 min, and their UV–vis spectra were recorded.

For kinetic measurements, the intensity at the steepest slope of the LSPR spectrum was monitored (**Figure S19**) following addition of the protein interaction partner, rather than recording the full spectrum, to enable higher temporal resolution. During data acquisition, the nanoparticle suspension was continuously stirred at 600 rpm.

Table S2. Protein-Protein Interaction pairs and corresponding sensing buffers

Entry	Protein Pair	Sensing Buffer
1	PEX52 / PEX14	20 mM Na_2HPO_4/NaH_2PO_4, 150 mM NaCl, 0.025% Tween-20, pH 7.5 - 7.9
2	PEX51 / PEX14	10 mM Tris, 50-150 mM NaCl, 0.025% Tween-20, pH 7.2 - 7.5
2	TAD / NCBD	10 mM Tris, 50-150 mM NaCl, 0.025% Tween-20, pH 7.2 - 7.5
3	TAD / MDM2	20 mM Na_2HPO_4/NaH_2PO_4, 150 mM NaCl, 0.025% Tween-20, pH 7.2
4	ACTR / NCBD	10 mM Tris, 50 mM NaCl, 0.025% Tween-20, pH 7.2
5	Biotin / Streptavidin	10 mM Tris, 50 mM NaCl, 0.025% Tween-20, pH 7.2

Table S3. Titrated concentrations for "Different PPIs" experiments (**Figures 3**e,f and **4**c,d). POI-1 was immobilized on nanosensors (via SPAAC or SML) and POI-2 was titrated. BSA control concentrations were matched to the corresponding protein concentrations.

Entry	Protein Pair (POI-1 / POI-2)	Concentration of titrated protein (POI-2)	Literature K_D values
1	PEX52 / PEX14	300 nM	139 - 344 nM (ITC)[6]
2	PEX51 / PEX14	300 nM	157 nM (ITC)[7], 87 nM (SPR)[7], 289 nM (LSPR)[1]
2	TAD / NCBD	270 nM[a]	3.3 μM (single-molecule FRET)[8]
3	TAD / MDM2	100 nM	100 nM (stopped-flow)[9]
4	ACTR / NCBD	100 nM	98 nM (ITC)[10]

[a]Note: for TAD/NCBD, a much lower concentration than the K_D was used in this study, since high concentrations of NCBD caused aggregation of the nanosensors, presumably due to the formation of NP oligomers.[1]

Table S4. Protein amino acid sequences of constructs used for PPI sensing experiments. Cysteine (C) and glycine (G) residues employed for site-specific maleimide labeling (followed by SPAAC) or sortase-mediated ligation are underlined.

Entry	Protein	Protein AA sequence	MW (kDa)
1	PEX52-C	**C**AMADLALSENWAQEFLAAGDAVDVTQDYNETDWSQEFISEVT DPLSVSPARWAEEYLEQSEEKLWLGEPEGTATDRWYDEYHPEEDL QHTASDFVAKVDDPKLANSEFLKFVRQIGEGQVSLE	14.12
2	PEX51-C	**C**AMAMRELVEAECGGANPLMKLAGHFTQDKALRQEGLRPGPW PPGAPASEAASKPLGVASEDELVAEFLQDQNAPLVSRAPQTFKMD DLLAEMQQIEQSNFRQAPQRAPGVADLA	12.33
3	PEX52-G	**G**AMADLALSENWAQEFLAAGDAVVDVTQDYNETDWSQEFISEV TDPLSVSPARWAEEYLEQSEEKLWLGEPEGTATDRWYDEYHPEED LQHTASDFVAKVDDPKLANSEFLKFVRQIGEGQVSLE	14.17
4	PEX51-G	**G**AMAMRELEAECGGAANPLMKLAGHFTQDKALRQEGLRPGPW PPGAPASEAASKPLGVASEDELVAEFLQDQNAPLVSRAPQTFKMD DLLAEMQQIEQSNFRQAPQRAPGVADLA	12.25
5	TAD-C	**C**AMEPLSQETFSDLWKLLPENNVLSPLPSQAMDDLMLSPDDIEQ WFTEDPGPD	6.01
6	TAD-G	**G**AMEPLSQETFSDLWKLLPENNVLSPLPSQAMDDLMLSPDDIEQ WFTEDPGPD	5.96
7	ACTR	**G**PGTQNRPLLRNSLDDLVGPPSNLEGQSDERALLDQLHTLLSNTD ATGLEEIDRALGIPELVNQGQALEPKQD**C**	7.96
8	NCBD	GAMEPPRSISPSALQDLLRTLKSPSSPQQQQQVLNILKSNPQLMAA FIKQRTAKYVANQPGMQ	6.93
9	MDM2	GAMAVPTDGAVTTSQIPASEQETLVRPKPLLLKLLKSVGAQKDTY TMKEVLFYLGQYIMTKRLYDEKQQHIVYCSNDLLGDLFGVPSFS VKEHRKIYTMIYRNLVVVNQQESSDSGTSVSEN	13.69
10	Sortase 4M	MKHHHHHHPMKQYKLILNGKTLKGETTTEAVDAATAEKVFKQY ANDNGVDGEWTYDDATKTFTVTEGSGSGSENLYFQSAMAKPQIP KDKSKVAGYIEIPDADIKEPVYPGPATSEQLNRGVSFAEENESLDD QNISIAGHTFIDRPNYQFTNLKAAKKGSMVYFKVGNETRKYKMT SIRNVKPTAVGGLEQKGKDKQLTLITCDDYNEKTGVWETRKIFVA TEVK	25.26
11	PEX14	GAMATPGSENVLPREPLIATAVKFLQNSRVRQSPLATRRAFLKKK GLTDEEIDMAFQQSGTAADEPSSLW	7.63

NP protein corona DLS characterization

AgDNP@Au nanoparticles were functionalized with either CysPoly(AEEA), following the procedure described in this manuscript, or PEG/NTA (80:20 ratio), following the methods reported by Zhou et al.[1] Functionalized particles were centrifuged twice for 10 min at 10,800 × g, and the resulting pellet was redispersed in Milli-Q (3 mL) water. Dynamic light scattering (DLS) measurements were performed in backscattering configuration using a ZetaSizer Ultra (Malvern Panalytical). Each measurement was repeated three times, and the data were averaged and plotted. For serum incubation, the particles were centrifuged for 10 min at 10,800 × g and redispersed in undiluted fetal bovine serum (350 µL). Samples were incubated on an orbital shaker at room temperature for 90 min. After incubation, particles were centrifuged and washed twice with Milli-Q water (500 µL) (10 min at 10,800 × g per wash). Finally, nanoparticles were redispersed in Milli-Q water (3 mL) and characterized by DLS.

Peak Shift Predictions

Refractive index (RI) sensitivity experiments were performed by exposing PEG/NTA- and CysPoly(AEEA)-functionalized nanoparticles to a series of glycerol–water mixtures, following the procedure described by Zhou et al.[1] The bulk RI values of the solutions were determined using a digital handheld refractometer (DR101-60, Krüss). The shift in the localized surface plasmon resonance peak position was plotted as a function of the RI change, and RI sensitivities (in meV/RIU) were obtained from the slopes of linear fits to the spectral shift versus RI variation. Nanoparticles functionalized with PEG/NTA exhibited an RI sensitivity of −926.32 meV/RIU, while CysPoly(AEEA)-functionalized nanoparticles showed a sensitivity of −791.95 meV/RIU. Using these sensitivities and the RI difference of 0.0099 between Milli-Q water (RI = 1.3329) and fetal bovine serum (FBS, RI = 1.3428), the expected LSPR shift arising solely from bulk RI changes was calculated. It should be noted that the RI sensitivities were determined using a different nanoparticle batch and may therefore be subject to batch-to-batch variations. Consequently, the calculated LSPR shifts are not intended to provide a strictly quantitative description, but rather to qualitatively demonstrate that PEG/NTA-functionalized nanoparticles exhibit substantial LSPR shifts upon exposure to FBS that cannot be explained by bulk RI changes alone.

Nanobiosensor Benchmarking using Biotin/Streptavidin interaction

The performance of the nanobiosensor platform was benchmarked and characterized using the well-established biotin–streptavidin interaction pair. For this purpose, DBCO-PEG_4-biotin (Sigma-Aldrich, 760749) was reacted with CysPoly(AEEA)$_7$ azido-alanine (**Table S1**). The resulting biotinylated conjugate was then grafted onto nanoparticles using a premix ratio of CysPoly(AEEA)$_4$ to biotin–CysPoly(AEEA) of 9:1, following the procedure described in the section *"Functionalization of AgDNP@Au Nanoparticles with POI–CysPoly(AEEA) Conjugates (via SPAAC or SML)"*. Binding and kinetic experiments were performed as described in *"Protei-Protein Interaction Sensing in Buffer/FBS"*, using streptavidin (Sigma-Aldrich, S4762).

Molecular Dynamic Simulations (methods)

Two gold surfaces were built using the CHARMM-GUI nanomaterial modeler[11] with dimensions of 100 Å × 100 Å × 10 Å and 140 Å × 140 Å × 10 Å, and were modified with a PEG-Thiol ligand with a surface coverage of 2 chains nm^{-2}. The systems were solvated with TIP3P water and 150 mM of NaCl. The CysPoly(AEEA) and NTA surface ligands were separately created with the CHARMM-GUI ligand builder.[12] Using a custom Python script, the PEG-Thiol ligands were fully or partially replaced at the sulfur–gold linkage to generate one surface fully modified with CysPoly(AEEA) and one surface with 60% PEG-Thiol and 40% NTA ligands, randomly distributed across the surface. For the larger surface, a BSA molecule (PDB ID 4F5S)[13,14] was prepared with the CHARMM-GUI PDB reader[15] and placed approximately 10 Å above the brush tips in three different orientations (**Figure S7**). All non-water components, including Ni^{2+} ions, were described with the CHARMM36 force field.[16] All gold atoms were permanently position-restrained at 1,000 kJ mol^{-1} nm^{-2} in all three dimensions throughout all simulation stages.

For all simulations, the Verlet cut-off scheme was employed. Van der Waals interactions were calculated using a cut-off with a force-switch modifier (r_{switch} = 1.0 nm, r_{vdw} = 1.2 nm). Electrostatic interactions were handled with Particle Mesh Ewald[17] with $r_{coulomb}$ = 1.2 nm. All bonds to hydrogen atoms were constrained with the LINCS algorithm[18]; water geometry was maintained with the SETTLE algorithm.

Energy minimization was performed using a steepest-descent algorithm for up to 5,000 steps or until convergence (ε_{max} = 1,000 kJ mol^{-1} nm^{-1}). The thiol sulfur anchor atoms of the surface ligand chains were harmonically restrained at 400 kJ mol^{-1} nm^{-2}.

NVT equilibration was run for 125 ps with a timestep of 1 fs, employing restraints (400 kJ mol^{-1} nm^{-2}) on the thiol sulfur anchor atoms of the surface ligand chains. The temperature was set at 300 K using a V-rescale thermostat[19] (τ_T = 1.0 ps) with separate coupling groups for the surface and the solvent. Initial velocities were generated from a Maxwell–Boltzmann distribution at 300 K.

Subsequently, an NPT equilibration was performed for 1 ns with a timestep of 2 fs. The thiol sulfur anchor atoms of the surface ligand chains were restrained (100 kJ mol^{-1} nm^{-2}). The temperature was controlled as described above. The pressure was controlled at 1 bar using a C-rescale barostat with semiisotropic coupling (compressibility = 0 bar^{-1} (surface-plane fixed), normal (z) compressibility = 4.5×10^{-5} bar^{-1}, τ_P = 5.0 ps).[20]

For the smaller surface, a 500 ns production run was performed in the NVT ensemble to study brush hydration, with a timestep of 2 fs and no restraints on the surface ligands. For the larger surface, a 10 ns production run was performed prior to the introduction of BSA. The temperature was controlled at 300 K as described above.

BSA adsorption was studied on both surface types (CysPoly(AEEA) and mixed NTA/PEG). Three initial orientations (A, B, C) of BSA relative to the surface were simulated for each surface type, yielding a total of 6 systems. For the mixed NTA/PEG surface, an additional set of three simulations was performed in which Ni^{2+} ions were placed at each NTA chelation site using a custom Python script, and harmonic Ni^{2+}–NTA distance restraints (disre-fc = 1000 kJ mol^{-1} nm^{-2}) were applied throughout all simulation stages to maintain Ni^{2+} chelation at the NTA sites.

The same minimization and equilibration protocol described above was applied, with the protein included as an additional thermostat coupling group. The protein backbone and sidechain heavy atoms were additionally restrained at 400 and 40 kJ mol^{-1} nm^{-2}, respectively, during minimization and NVT equilibration. Production runs were performed in the NVT ensemble for up to 1000 ns with a timestep of 2 fs and no position restraints on the surface ligands or protein.

All simulations were performed with GROMACS 2025.2.[21,22] Trajectory analysis was performed with MDAnalysis[23,24], and structures were visualized and rendered with ChimeraX[25] or PyMOL[26].

BSA–Surface Contact Classification

To characterize the nature of BSA adsorption, contacts between BSA residues and the surface brush were classified into five interaction types based on geometric criteria applied throughout each trajectory. Salt bridges were identified between acidic BSA residues (Asp/Glu) and surface Ni^{2+} ions (heavy-atom distance $\leq$ 4 Å), and between basic residues (Lys/Arg) and NTA carboxylate oxygens (distance $\leq$ 4 Å).[27] Hydrogen bonds were assigned using a donor–hydrogen···acceptor distance cut-off of 2.5 Å and a minimum angle of 120°,[28] distinguishing three sub-types: BSA donating to NTA carboxylate acceptors, BSA donating to any brush acceptor atom, and brush chains donating to BSA acceptor atoms. Contacts were further classified as persistent (survival fraction $C(\tau)$ still active at τ = 100 ns) or transient (contacts that formed but dissipated before 100 ns), providing a measure of contact stability over the simulation timescale. Persistent contacts were used as the primary metric for comparing adsorption across surface types and orientations, as they reflect interactions that persist on the hundred-nanosecond timescale and are therefore more indicative of stable, long-lived protein binding than transient contacts (**Figure 1g**).

A distinction was made between ionic contacts and hydrogen bonding (**Figure S**5), as these two classes differ fundamentally in both their physical origin and binding strength: Ni^{2+}-mediated salt bridges, which involve direct metal–carboxylate coordination, carry a substantially higher binding free energy ($\Delta G° \approx -3$ to -12 kcal/mol depending on coordination geometry)[29] than hydrogen bonds or carboxylate–Lys/Arg salt bridges ($\Delta G° \approx -1$ to -5 kcal/mol).[30,31] On the mixed NTA/PEG surface, ionic contacts are both more numerous and individually stronger than hydrogen bonds, suggesting that Ni^{2+} chelation sites drive BSA adsorption through a combination of contact frequency and interaction strength.

Brush Hydration

To assess the hydration state of the two brush types independently of BSA, water–ligand hydrogen bonds per chain were monitored over 500 ns NVT simulations of the bare surfaces (without protein). Separate time series were extracted for NTA and PEG chains on the mixed surface, as well as for the CysPoly(AEEA) chains (**Figure S6**), and are reported as the mean number of H-bonds per chain per frame at 1 ns resolution. For the mixed surface, a composite hydration metric was computed as a weighted average of the PEG and NTA contributions (60% and 40% by chain composition, respectively). These data characterize the equilibrium solvation shell of each brush type and provide a baseline for interpreting changes in surface hydration upon BSA adsorption. The sustained hydration of both brush types throughout the simulations is consistent with the known hydrophilicity of PEG[32] and the coordination environment of NTA,[33] and supports the view that water displacement represents the thermodynamic cost associated with protein adsorption.[34]

Quantification of CysPoly(AEEA)$_4$ and PEX52-CysPoly(AEEA)$_7$ Surface Coverage by Supernatant Depletion Assay

Surface ligand density was quantified for both CysPoly(AEEA)$_4$ and the protein conjugate PEX52-CysPoly(AEEA)$_7$ by a supernatant depletion assay using Ellman's reagent (5,5′-dithiobis-(2-nitrobenzoic acid), DTNB), which reacts stoichiometrically with free thiols to produce the chromogenic TNB^{2-} anion, quantifiable by absorbance at 412 nm (ε = 14,150 $M^{-1}cm^{-1}$).[35] The two ligands were assayed in independent experiments following the same protocol with different batches of AgDN@Au's. For coupling of PEX52 and CysPoly(AEEA)$_7$-azido-alanine PEX52 was firstly labeled with DBCO via Maleimide conjugation chemistry and then "clicked" to the CysPoly(AEEA)$_7$-azido-alanine. For details refer to "Protein Maleimide-DBCO modification" and "Strain-Promoted Azide–Alkyne Cycloaddition (SPAAC) Between POI–DBCO and CysPoly(AEEA)-Aza-Amide".

AgDNP@Au nanoparticles were prepared for ligand conjugation as described in Section "Functionalization of AgDNP@Au Nanoparticles with POI-CysPoly(AEEA) Conjugates", with the modification that a 10-fold higher NP concentration was used to ensure measurable ligand depletion. To this end, ten 289 µL aliquots of NP suspension (extinction 1.4 at λ_{LSPR}) were centrifuged (10 min, 10,800 × *g*), the supernatants discarded, and the residual pellet volume recorded. The combined pellet was resuspended in 20 µL of the respective ligand solution (either CysPoly(AEEA)$_4$ or PEX52-CysPoly(AEEA)$_7$) and brought to a final volume of 300 µL with assay buffer (10 mM Tris, 50 mM NaCl, 1 mM EDTA, 0.025% Tween-20, pH 7.5), chosen to satisfy both NP colloidal stability and DTNB assay compatibility. Three samples were prepared in parallel for each ligand: (1) NP + ligand (depletion sample), (2) ligand in buffer only (reference), and (3) buffer only (blank). Samples 2 and 3 were assayed immediately to establish the initial thiol concentration; all three samples were then incubated overnight at 4 °C.

Following incubation, sample 1 was centrifuged (10 min, 10,800 × g) to pellet the nanoparticles, and the supernatant was recovered. All samples (supernatants and references) were assayed by

mixing 90 µL of sample with 10 µL of 4 mM DTNB solution, incubating for 15 min at room temperature, and measuring absorbance at 412 nm. The free thiol concentration in each sample was calculated from the TNB^{2-} absorbance using the Beer-Lambert law and the extinction coefficient above. The amount of surface-bound ligand was determined from the difference in thiol concentration between the ligand reference (sample 2) and the NP supernatant (sample 1). In both cases, the measured depletion corresponds directly to surface-bound ligand molecules in a 1:1 stoichiometry: CysPoly(AEEA)$_4$ carries a single terminal cysteine as its sole reactive thiol, and PEX52-CysPoly(AEEA)$_7$ carries the same unique thiol through the conjugate (PEX52 contains no solvent-exposed cysteine residues, **Table S4**), with free unconjugated CysPoly(AEEA)$_7$ removed by successive concentrator column washes (Amicon Ultra 3kDa 0.5mL) prior to the assay to reduce contributions of false positives. In addition to the Ellman's assay, the UV spectra of incubated PEX52-CysPoly(AEEA)$_7$ samples were measured (prior to DTNB addition) to directly determine the protein depletion based on the high extinction coefficient of the PEX52 at 280nm (33,585 $M^{-1}cm^{-1}$) yielding a protein grafting density of 0.14 ligands/nm^2 respectively (**Figure S17**).

AgDNP@Au particle concentration was estimated from the $AgNO_3$ mass balance as described previously,[1] assuming full conversion of the precursor to pentagonal bipyramidal AgDNPs and accounting for the 1:1 dilution during Au shell deposition, yielding a final NP concentration of 1 nM (0.8 nM in PEX52-CysPoly(AEEA)$_7$ experiment) in the depletion assay suspension. The particle surface area (3.04×10^3 nm^2 per particle) was taken from the same reference, calculated by modelling each particle as a pentagonal bipyramid with equilateral triangular faces and an edge length of 26.5 nm as determined by TEM. The grafting density σ was calculated as:

$$\sigma = \frac{[ligand]_{bound}}{[AgDNP@Au] \times A_{AgDNP@Au}} = \frac{[ligand]_{bound}}{[AgDNP@Au] \times 3040\ nm^2},$$

where $[ligand]_{bound}$ corresponds to the thiol concentration depletion measured by the Ellman's assay, $[AgDNP@Au]$ to the estimated particle concentration and $A_{AgDNP@Au}$ to the surface area per particle. The depletion assay yielded 6700 ligands/particle for protein unmodified CysPoly(AEEA) (**Figure S16**) and 2700 ligands/particle for PEX52 modified CysPoly(AEEA)$_7$ (**Figure S17**), which corresponds to grafting densities of 2.20 ligands/nm^2 and 0.9 ligands/nm^2 respectively; direct UV quantification of the same supernatant gave 430 proteins per particle (0.14 proteins/nm^2). See Supplementary Discussion for interpretation of the two values.

Comparison of CysPoly(AEEA)$_4$ and SH-PEG800 NP grafting

Nanoparticle pellets, prepared identically as described in "Functionalization of AgDNP@Au Nanoparticles With POI–CysPoly(AEEA) Conjugates", were redispersed in MilliQ water, and CysPoly(AEEA)$_4$ (MW = 742 Da) or SH-PEG800 (Sigma-Aldrich, 729108, MW ~ 800 Da) was added to reach a final ligand concentration of 110 µM in a total volume of 350 µL. The ligand grafting process was monitored by UV-vis extinction measurements (**Figure S8**a, b).

Comparison of CysPoly(AEEA)$_5$-N$_3$ and SH-PEG-N$_3$

To compare the effect of CysPoly(AEEA) on the overall sensing performance, nanoparticles were functionalized with azide-containing CysPoly(AEEA)$_5$-N$_3$ (MW = 1000 Da) or SH-PEG-N$_3$ (MW ~1000 Da) and characterized via UV-vis extinction measurements (**Figure S8**c). Note that a 1:1 ratio of azide-containing ligand to non-azide-containing ligand — CysPoly(AEEA)$_4$ (MW = 742) or SH-PEG800 (MW ~800 Da), respectively — was used to enhance colloidal stability of the sensors while facilitating comparison of CysPoly(AEEA)$_5$-N$_3$ and SH-PEG-N$_3$ ligands. To nanoparticle pellets, prepared identically as described in "Functionalization of AgDNP@Au Nanoparticles With POI–CysPoly(AEEA) Conjugates," 10 μL of a 1:1 premix of either 1 mM CysPoly(AEEA)$_5$-N$_3$: CysPoly(AEEA)$_4$ or 1 mM SH-PEG-N$_3$ (MW ~1000 Da) : SH-PEG800 (MW ~800 Da) was added; samples were incubated overnight, and the UV-vis spectrum was measured without additional centrifugation to avoid aggregation.

Sensing performance was assessed via the figure of merit (FOM), a standard metric for plasmonic sensors defined as the refractive index (RI) sensitivity normalized by the spectral linewidth of the LSPR resonance: $FOM = \frac{RI\ sensitivity\ (meV/RIU)}{LSPR\ FWHM\ (meV)}$, where FWHM is the full width at half maximum of the LSPR extinction peak.[36] A higher FOM reflects a sharper, more resolvable spectral shift per unit change in refractive index, and thus greater sensing capacity. Assuming constant RI sensitivity, a reasonable assumption for a single nanoparticle synthesis batch, the FOM scales inversely with FWHM, such that any broadening of the LSPR linewidth directly and linearly decreases sensing performance.

SUPPLEMENTARY Discussion

Quantification of CysPoly(AEEA)$_4$ surface coverage

Surface ligand coverage was quantified by an Ellman's reagent (DTNB) supernatant depletion assay, measuring the fraction of Cys-poly(AEEA)$_4$ bound to the nanoparticle surface after conjugation (**Figure S16**). At a nanoparticle concentration of 1 nM, the measured surface-bound ligand concentration was 6.7 μM, corresponding to 6,700 ligands per particle and a grafting density of 2.20 ligands/nm^2. The all-atom MD simulations presented in this work employed a surface density of 2.0 ligands/nm^2, in close agreement with this experimentally determined value.

This grafting density is consistent with values reported for thiol-terminated PEG and short thiol-linker systems on gold nanoparticles, although a direct comparison is complicated by differences in ligand molecular weight. Rahme et al. reported 3.93 ligands/nm^2 for mPEG-SH (MW 2,100 Da) on 15 nm AuNPs by thermogravimetric analysis,[37] and Hinterwirth et al. determined 4.29 ligands/nm^2 for short-chain PEG thiols (7-mer repeat) on AuNPs of 12–26 nm by ICP-MS.[38]

Two factors contribute systematic uncertainty to the value reported here. First, the nanoparticle concentration is derived from a mass-balance calculation assuming full conversion of the precursors to nanoparticles; incomplete conversion or batch-to-batch variability in synthesis yield therefore propagates directly into the calculated grafting density. Second, the ligand-to-particle ratio used in the depletion assay (~15,000–30,000 ligands per particle) is approximately 10-fold lower than under standard conjugation conditions, as the particle concentration was raised 10-fold to generate a measurable depletion signal. This reduced ratio may limit surface saturation and thus underestimate the maximum achievable grafting density. Conversely, the assay employed an overnight incubation, which is longer than the 1 h incubation used for nanosensor assembly. The value of 2.20 ligands/nm^2 is therefore best interpreted as a lower bound on the maximum achievable grafting density rather than as the exact coverage present during the binding measurements. At this density the mean interchain spacing is ~0.7 nm, comparable to the unperturbed dimensions of the ~750 Da ligand, placing the Cys-poly(AEEA)$_4$ layer in the dense brush regime expected to confer steric repulsion against non-specific protein adsorption and to support colloidal stability in complex biological media.[39]

Quantification of protein (PEX52–CysPoly(AEEA)$_7$) surface coverage

The number of proteins immobilised per nanoparticle influences both binding and sensing performance,[40] and was therefore quantified for the PEX52–Cys-poly(AEEA)$_7$ conjugate by two independent methods on the same sample (**Figure S**17).

The primary estimate was obtained by direct UV quantification of the protein. PEX52 has a molar extinction coefficient at 280 nm of 33,585 M^{-1}cm^{-1}, allowing the protein concentration depleted from the supernatant upon nanoparticle conjugation to be determined directly, independently of the thiol chemistry used for ligand quantification. This yielded a surface loading of 430 proteins per particle, corresponding to a grafting density of 0.14 proteins/nm^2. This value corresponds to a mean lateral footprint of ~7 nm^2 per protein, consistent with the dimensions expected for a ~14 kDa domain and therefore physically self-consistent. It is also in reasonable agreement with literature values for globular proteins on gold nanoparticles once molecular weight is accounted for: Kozlowski et al. reported 0.064–0.090 proteins/nm^2 for the globular enzyme DHFR (21 kDa).[41] The ~1.5–2-fold higher density measured here is consistent with the smaller size of PEX52 and with the fact that PEX52(110–230) is an intrinsically disordered region of PEX5,[6] which is expected to adopt a more extended, laterally compact configuration than a folded protein of comparable mass.[42]

For completeness, the same samples were also assayed by DTNB supernatant depletion using the protocol applied to the unmodified ligand. This returned 2,700 constructs per particle (0.90 proteins/nm^2). This value is not regarded here as an accurate measure of protein grafting density. The DTNB assay reports on thiol depletion rather than protein depletion. Residual unconjugated Cys-poly(AEEA)$_7$-N$_3$ is not quantitatively removed by concentrator washing and carries the same reactive thiol; its depletion onto the nanoparticle surface is therefore indistinguishable from protein depletion, inflating the apparent protein loading. Consistent with an overestimate, 0.90

proteins/nm^2 would imply a footprint of ~1.1 nm^2 per protein — smaller than the cross-section of the protein itself — and would require ~40% of all surface anchoring sites to carry a ~14 kDa construct, which is incompatible with the steric limitations on surface conjugation noted in the main text. The DTNB-derived value is therefore reported as an upper bound, and 0.14 proteins/nm^2 is taken as the best estimate of protein surface coverage.

As for the ligand-only measurement, the nanoparticles used for both assays were prepared at elevated particle concentration to give a measurable depletion signal, and their preparation differs from that used for the binding experiments in the main figures, where nanoparticles were incubated with PEX52–Cys-poly(AEEA)$_7$ for 1 h, backfilled with Cys-poly(AEEA)$_4$ for a further 1 h, and then purified. The reported values should accordingly be understood as an estimate of the achievable protein loading rather than the exact coverage present during the binding measurements.

SUPPLEMENTARY FIGURES

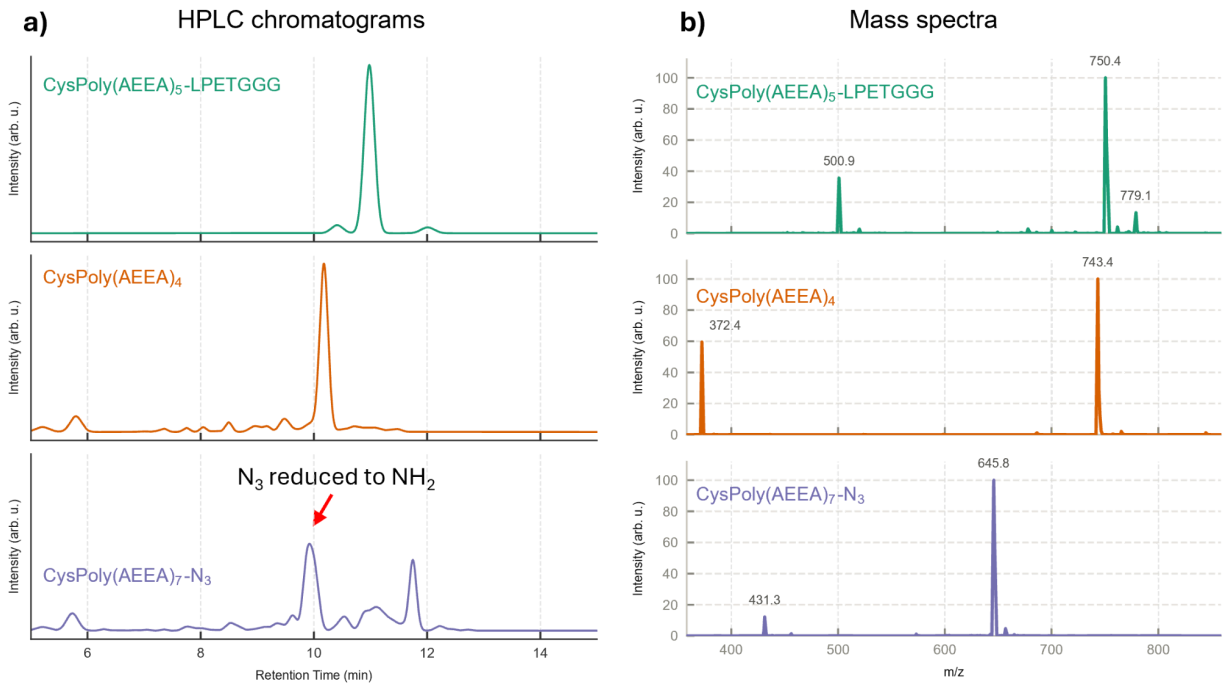


Figure S1: a) HPLC and b) mass-spectrometry characterization of Cys-Poly(AEEA) antifouling ligands used in this manuscript: CysPoly(AEEA)$_5$-LPETGGG for SML (teal), CysPoly(AEEA)$_4$ for backfilling (orange), and CysPoly(AEEA)$_7$-N$_3$ for SPAAC (purple). CysPoly(AEEA)$_4$ and CysPoly(AEEA)$_7$-N$_3$ were stored under reducing conditions prior to measurement (TCEP, to prevent disulfide formation), which as an unintended side effect partially reduced the azide of CysPoly(AEEA)$_7$-N$_3$ to an amine. Consequently, the HPLC trace for CysPoly(AEEA)$_7$-N$_3$ shows two peaks: one at 10 min corresponding to the reduced (NH$_2$) form and one at 11.8 min corresponding to the intact (N$_3$) form.This reduction occurred only in samples for these measurements; ligands used for nanoparticle functionalization were not exposed to TCEP. In b) For Cys-Poly(AEEA)$_5$-LPETGGG and Cys-Poly(AEEA)$_7$-N$_3$, the peaks at m/z 750.4 and 645.8, respectively, correspond to the $[M+2H]^{2+}$charge state of the ligand. For Cys-Poly(AEEA)$_4$, the peak at m/z 743.3 corresponds to the $[M+H]^{+}$ charge state.

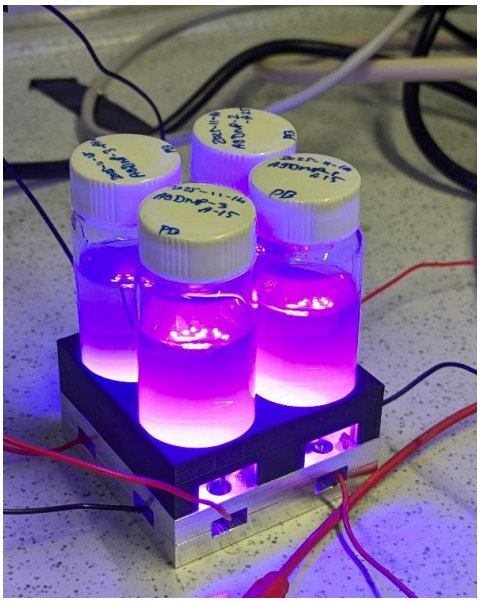


Figure S2: Image of a home-built photoreactor used for the synthesis of AgDNP, showing four example reaction vials containing AgDNP precursor solutions. Each LED is powered by a separate channel of a laboratory power supply.

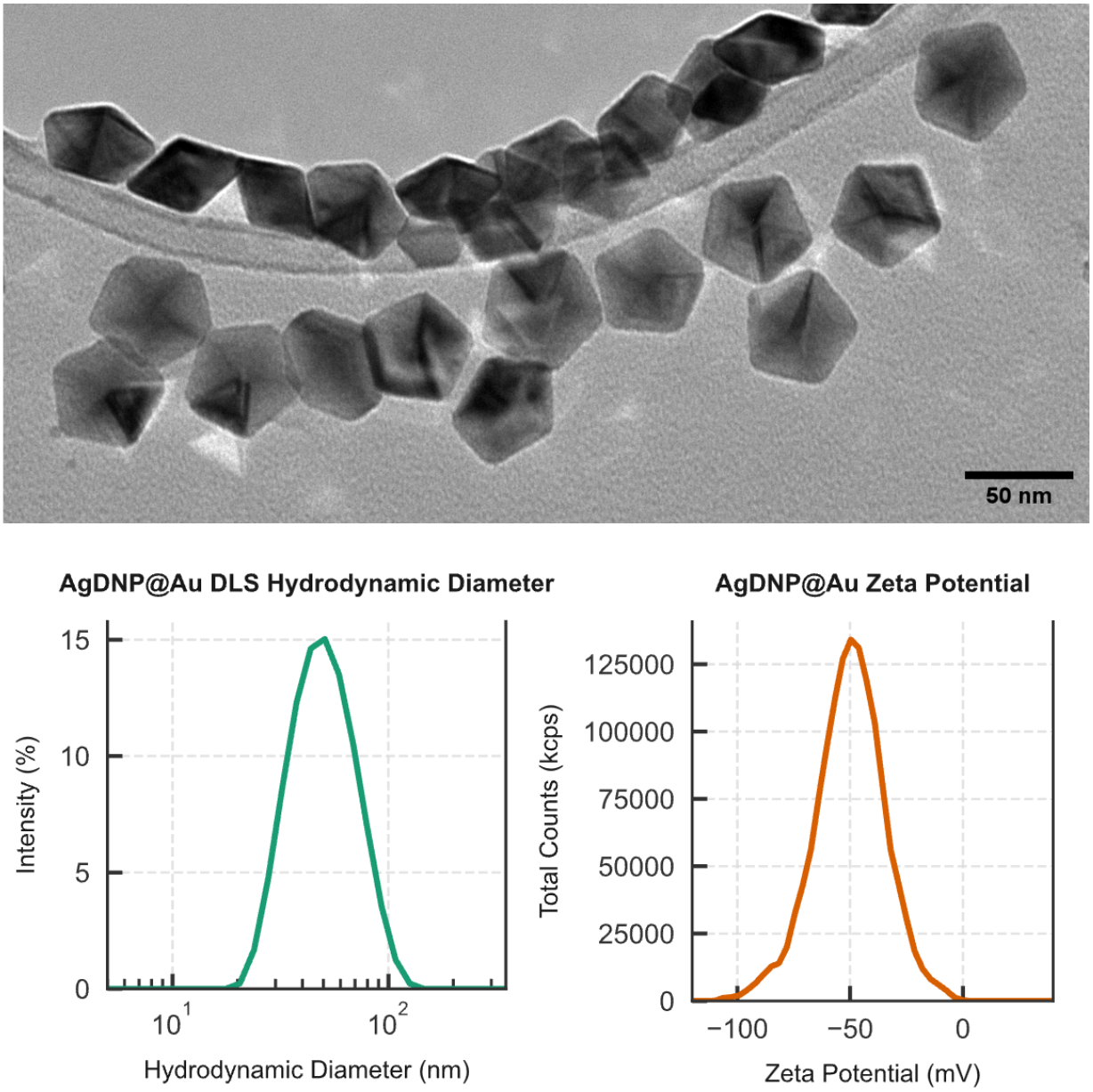


Figure S3: Characterization of gold-coated silver decahedral nanoparticles (AgDNP@Au). (Top) TEM micrograph of AgDNP@Au. (Bottom left) Hydrodynamic diameter distribution measured by DLS. (Bottom right) Zeta potential distribution of AgDNP@Au.

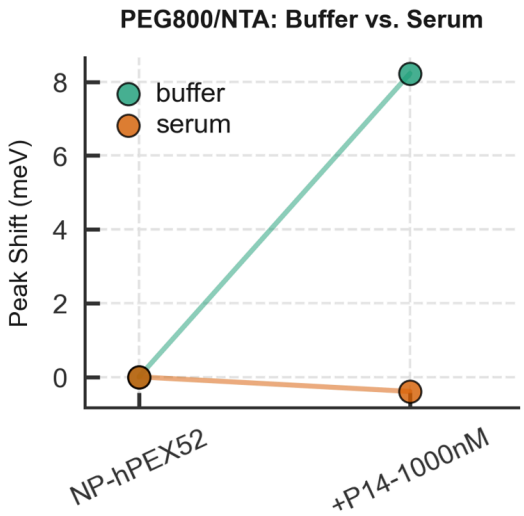


Figure S4: Scatterplot illustrating the LSPR peak shift of modified nanobiosensors following the addition of His-PEX52 in sodium phosphate buffer and undiluted FBS. Upon subsequent addition of PEX14 (final concentration 1 µM), no significant LSPR shift was observed in FBS, whereas a pronounced shift was detected under buffer conditions. These results indicate that pre-functionalization with the first protein prior to FBS exposure does not preserve sensor integrity in FBS.

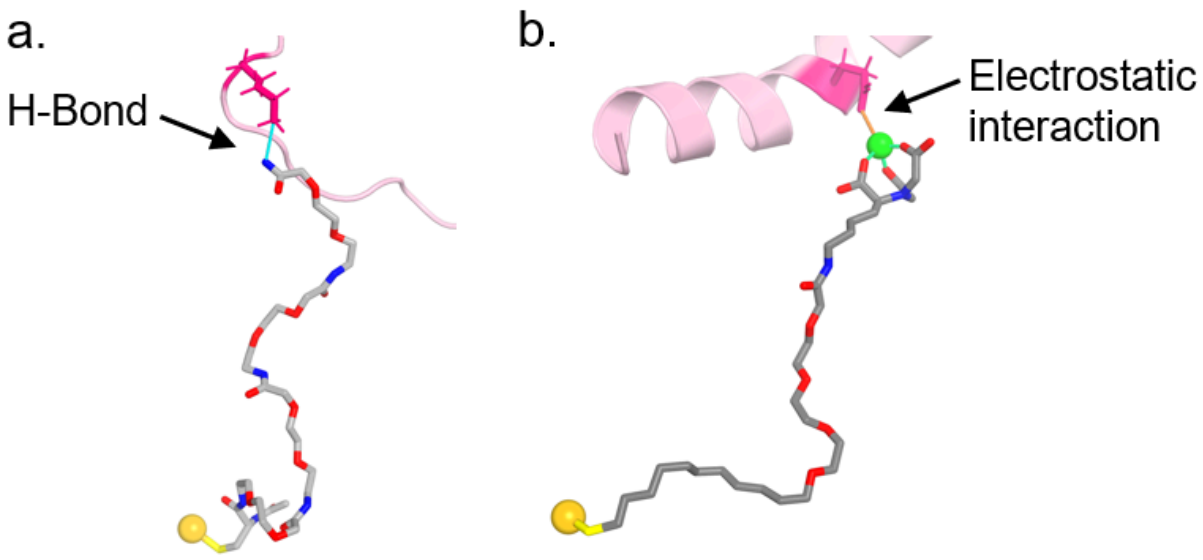


Figure S5: Molecular visualization renders generated with PyMOL. (a) Exemplary hydrogen-bond interactions of the Cys–Poly(AEEA) ligand with BSA. (b) Exemplary interaction of NTA/Ni^{2+} ligand with BSA. BSA is shown as pink cartoon/sticks; Ni^{2+} as a green sphere; Au as a yellow sphere; and NTA as sticks colored gray (carbon), red (oxygen), blue (nitrogen), and yellow (sulfur).

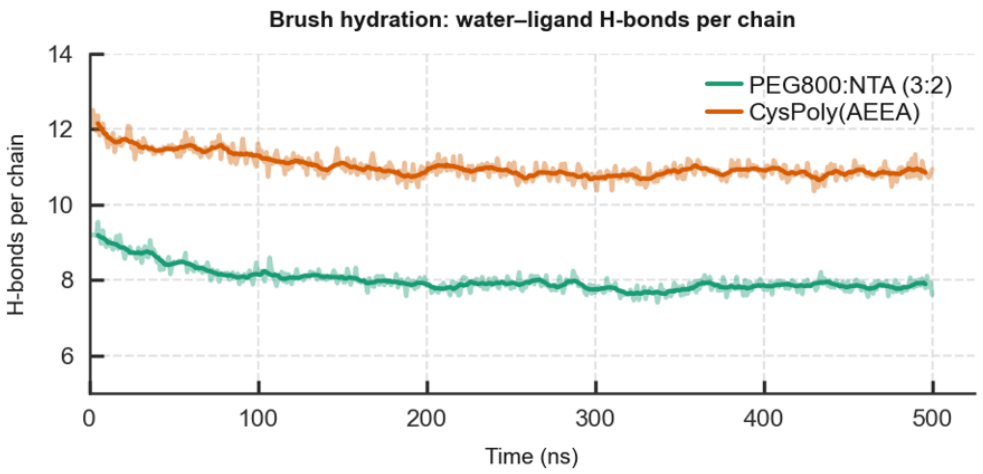


Figure S6: Time trace (light shading) and rolling average (darker shading) of the number of hydrogen bonds with water per surface brush for Cys–Poly(AEEA)-modified and PEG800-thiol/NTA–Ni^{2+}-modified gold surfaces over a 500 ns MD simulation.

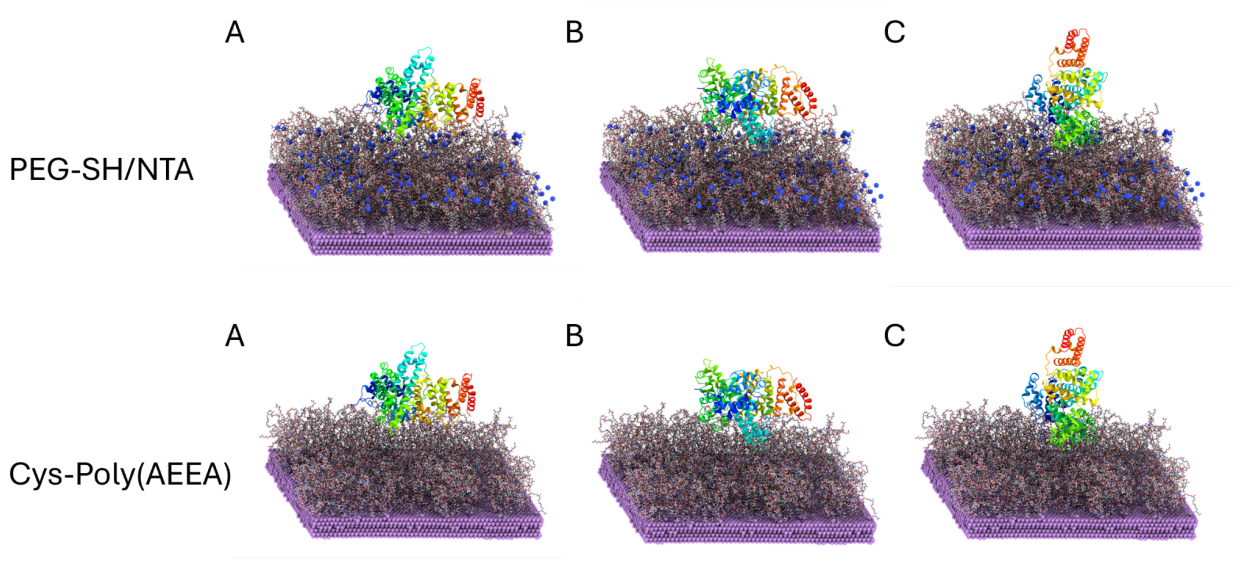


Figure S7: Molecular visualization renders generated with ChimeraX. Initial structures for MD simulation of mixed PEG-Thiol/NTA (top) and CysPol(AEEA) surfaces for three BSA orientations (A, B and C). The BSA molecule was placed roughly 10 Å above the surface brushes. The same orientations were used for the CysPoly(AEEA) modified surface. BSA is shown as a cartoon representation with rainbow coloring from C- to N-terminus. Gold atoms are shown as purple spheres, Ni^{2+} ions as blue spheres. Surface ligands are shown as sticks.

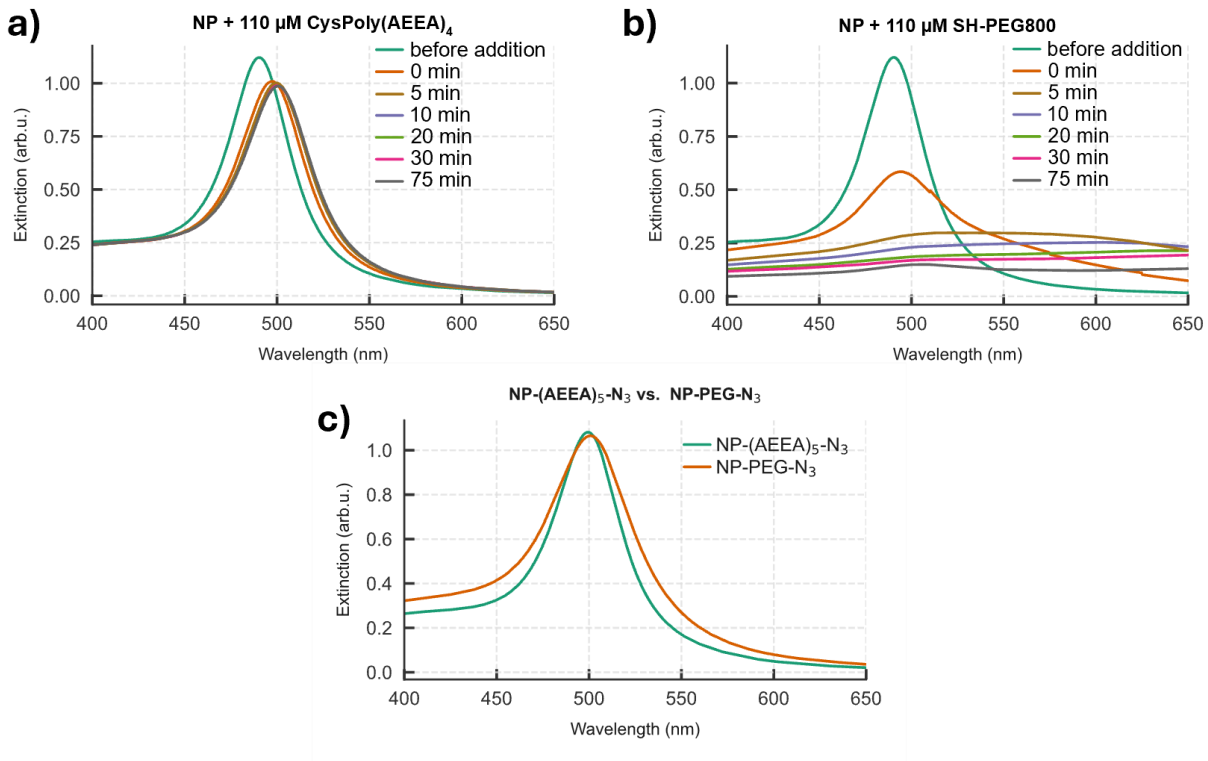


Figure S8: UV–vis spectra of bare AgDNP@Au nanoparticles after addition of a) 110 µM CysPoly(AEEA)$_4$ (MW = 742 Da) or b) 110 µM SH-PEG800 (MW ≈ 800 Da). Addition of SH-PEG800 induces clear spectral signatures of aggregation, whereas CysPoly(AEEA)$_4$ yields colloidally stable nanoparticles. c) UV–vis spectra of NPs modified with CysPoly(AEEA)$_5$-N$_3$ (MW = 1000.4 Da, teal) and SH-PEG-N$_3$ (NANOCS, PG2-AZTH-1k, MW ≈ 1 kDa, orange). Note that a 1:1 premix of the azide ligands and backfilling ligands without azide (CysPoly(AEEA)$_4$ and PEG800, respectively) was added to enhance colloidal stability without compromising the comparison of the ligand types. The significantly broader LSPR spectrum of the PEG-N$_3$-modified NPs (FWHM = 306 meV) compared to the CysPoly(AEEA)$_5$-N$_3$-modified NPs (FWHM = 237 meV) results in a 23% decrease in figure of merit, assuming constant refractive index sensitivity.

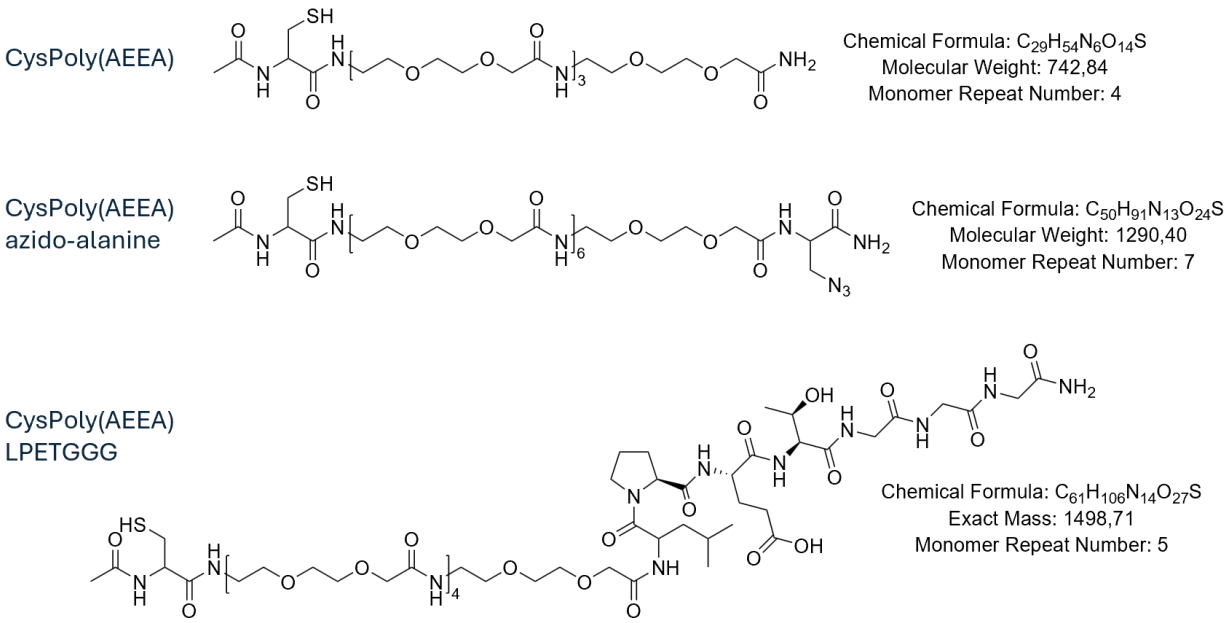


Figure S9: Chemical structures, formulas, molecular weights and monomer repeat numbers of the CysPoly(AEEA) antifouling ligands used in this manuscript (**Table S1**).

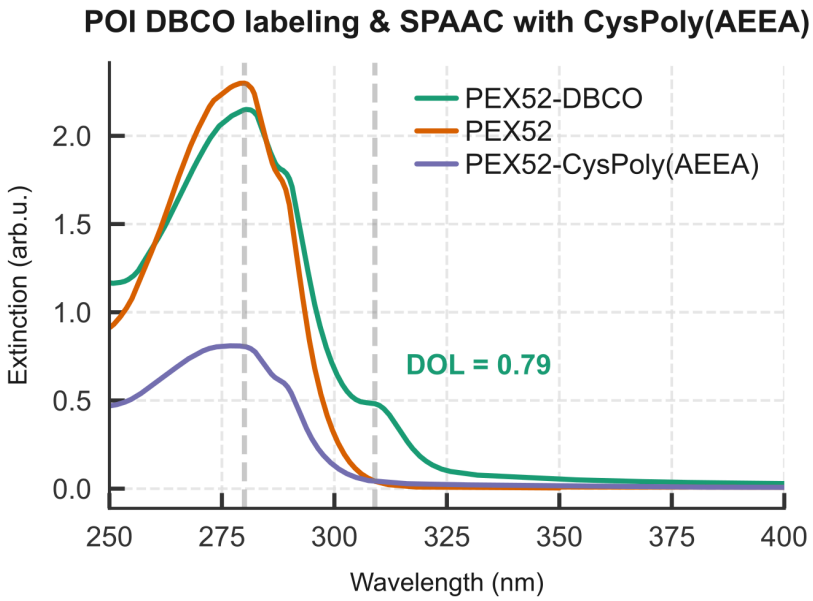


Figure S10: UVVis spectrum of the Cysteine-PEX52 protein before (orange) and after (teal) DBCO-PEG-maleimide labeling. A degree of labeling of 0.79 was calculated from the A280 of the protein and the A309 of the DBCO moiety. The purple spectrum corresponds to the product of the SPAAC reaction between PEX52-DBCO and CysPoly(AEEA) ligands. Complete conversion is indicated by the disappearance of the DBCO absorption peak at 309 nm, as the reaction product is non-absorptive at this wavelength.

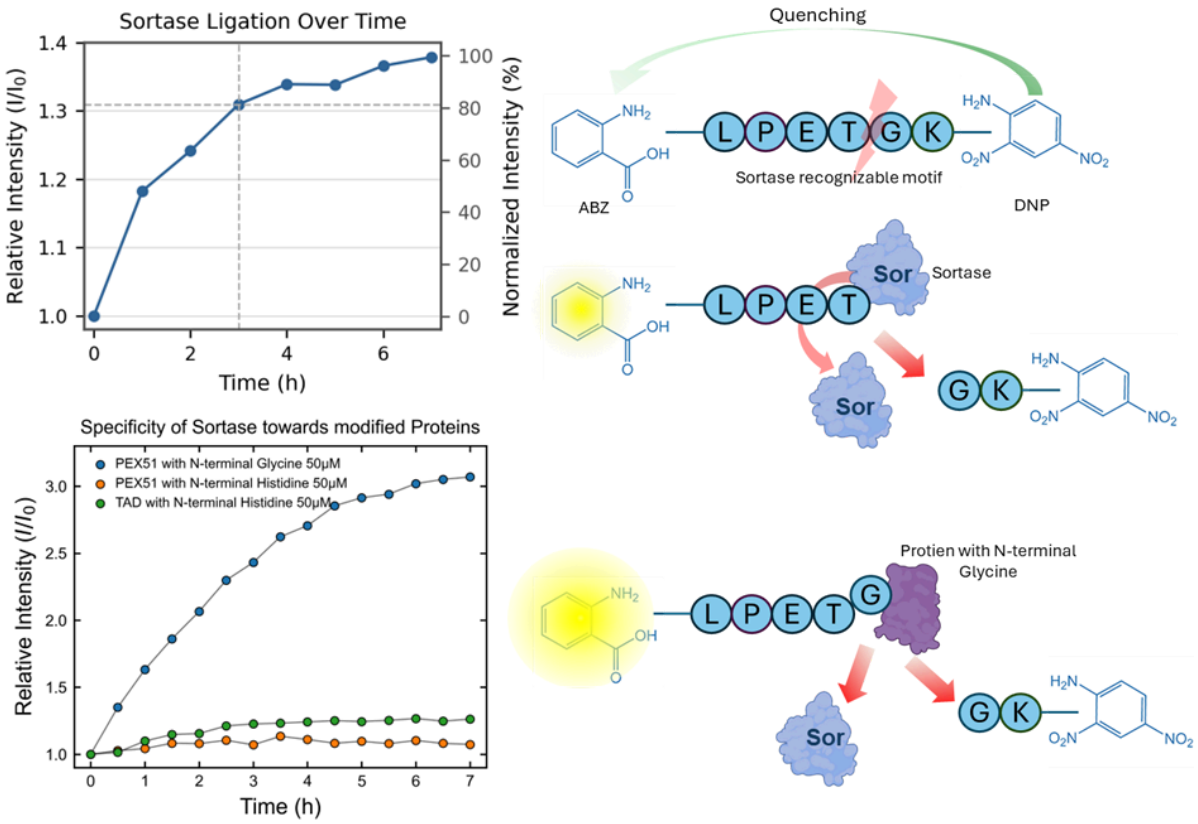


Figure S11: Illustration of a FRET-based sortase activity assay, demonstrating (top) enzymatic efficiency by measuring the time required to reach maximal ligation at 4 °C in a bacterial sortase system, and (bottom) ligation specificity, showing that a glycine-modified protein serves as an effective nucleophile compared to non-glycine controls and background hydrolysis.

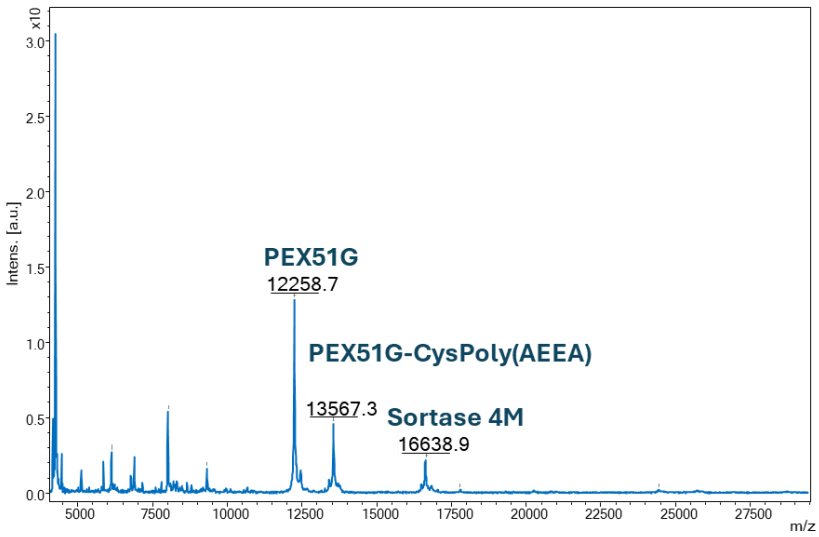


Figure S12: MALDI-TOF mass spectra confirming successful sortase-mediated ligation of PEX51 with CysPoly(AEEA). Peaks corresponding to the individual components and the resulting CysPoly(AEEA)–PEX51 conjugate are observed, with their respective molecular weights indicated in the figure.

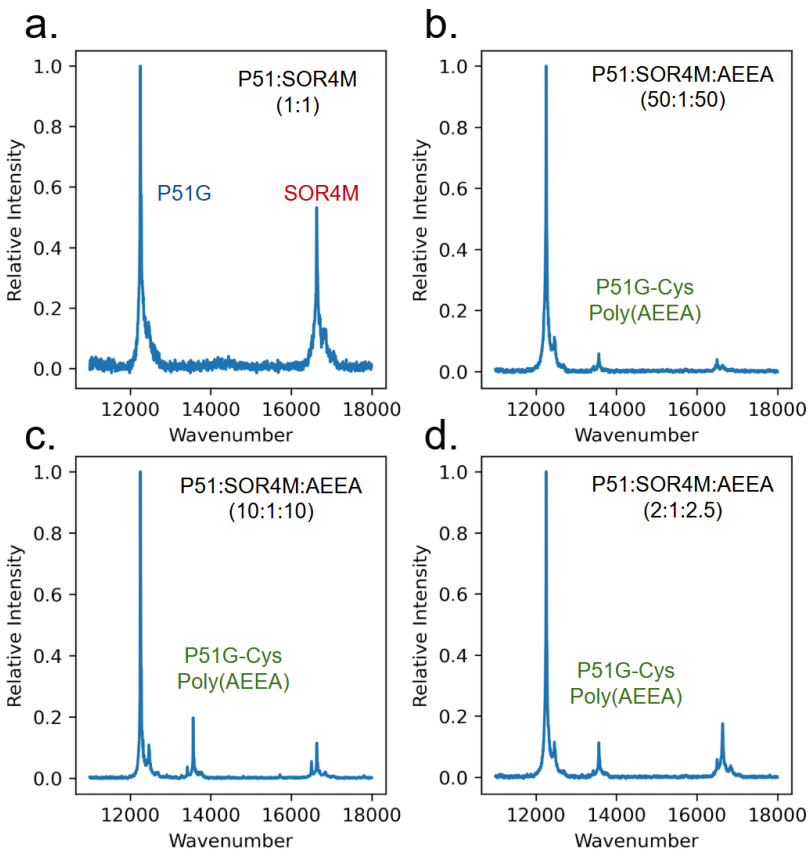


Figure S13: Normalized MALDI-TOF mass spectra demonstrating successful sortase-mediated ligation of PEX51 with CysPoly(AEEA). Four subplots show reactions performed under different molar ratios: (a) without CysPoly(AEEA), (b) 50:1:50, (c) 10:1:10, and (d) 2:1:2.5. The control sample (without CysPoly(AEEA)) shows no peak corresponding to the conjugated product, confirming the absence of ligation. In contrast, reactions containing CysPoly(AEEA) exhibit peaks corresponding to the CysPoly(AEEA)–PEX51 conjugate, with the 10:1:10 condition yielding the highest signal intensity, indicating the most efficient ligation under these conditions.

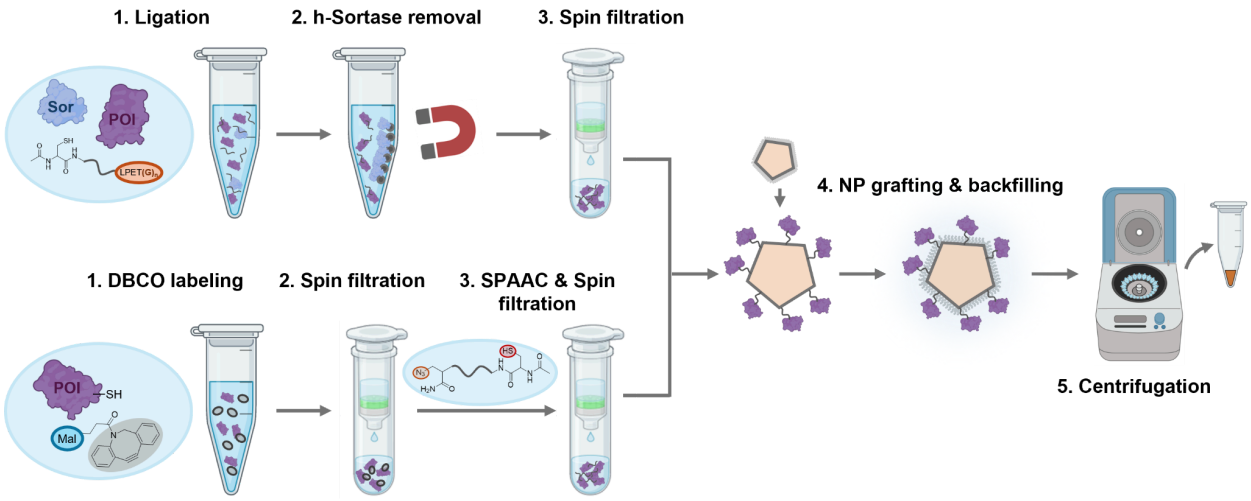


Figure S14: Workflow for preparing nanobiosensor constructs using both sortase-mediated ligation (SML, top) and strain-promoted azide–alkyne click chemistry (SPAAC, bottom).

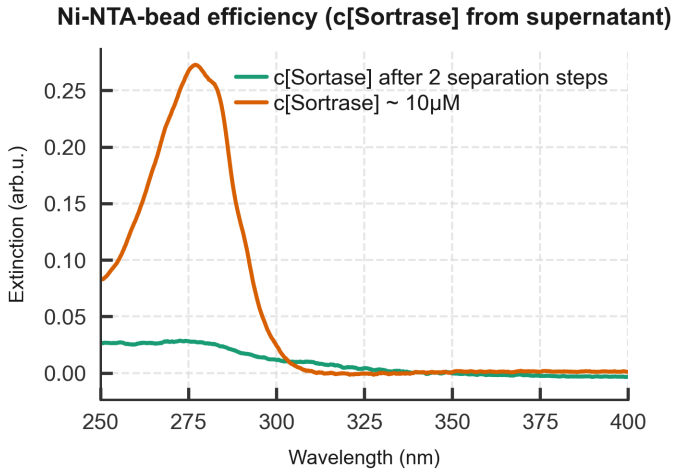


Figure S15: Removal of sortase after reaction using magnetic Ni-NTA beads. Results show efficient removal of His-tagged sortase from the solution.

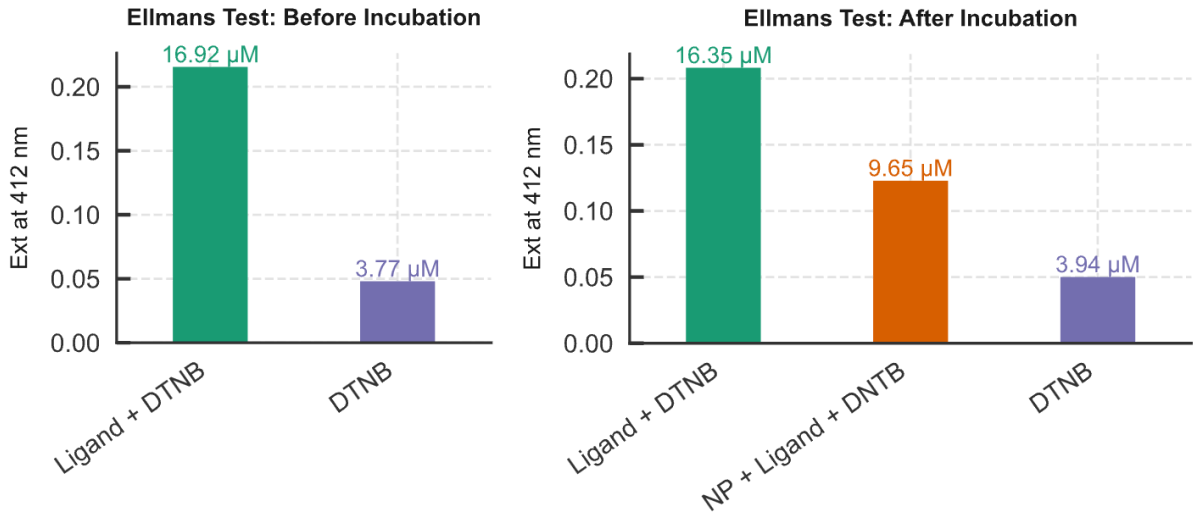


Figure S16: Ellman's (DTNB) supernatant depletion assay for quantification of Cys-poly(AEEA)$_4$ ("Ligand" in plots) surface loading on AgDNP@Au. Bars show free thiol concentration determined from absorbance at 412 nm before (left) and after (right) overnight incubation with AgDNP@Au (~1 nM). The overnight ligand-only control (teal, right) serves as the depletion reference to account for partial thiol oxidation during incubation. The bound ligand concentration is determined from the difference between the ligand-only control and the NP supernatant (orange), yielding 6.7 µM corresponding to ~6,700 ligands per particle. See "Quantification of CysPoly(AEEA)$_4$ and PEX52-CysPoly(AEEA)$_7$ Surface Coverage by Ellman's Reagent Depletion Assay" full experimental details.

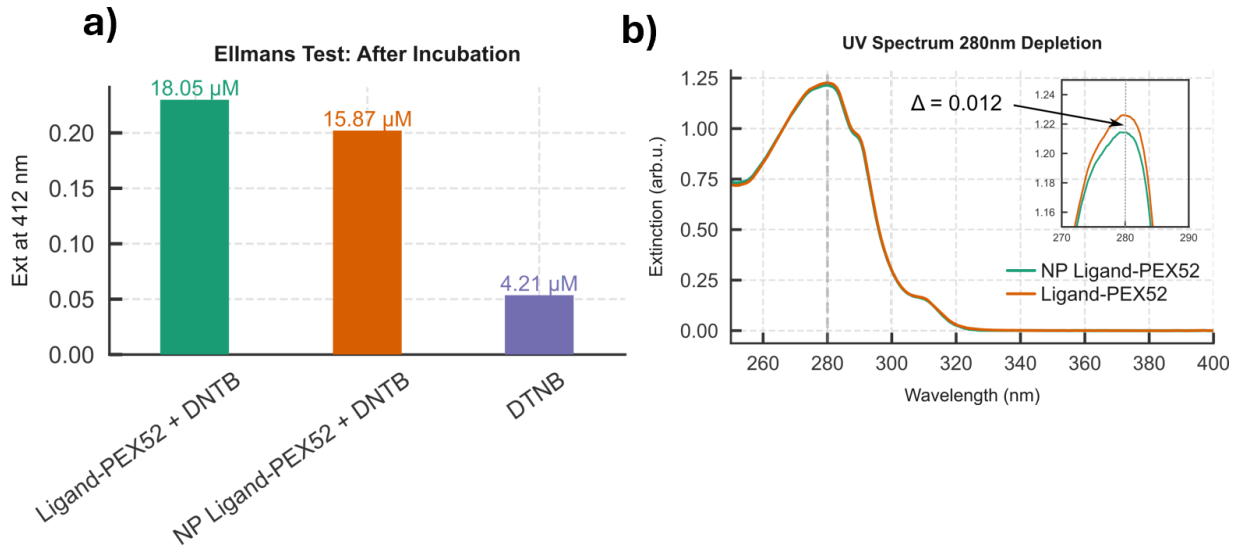


Figure S17: Ellman's (DTNB) supernatant depletion assay for quantifying PEX52-Cys-poly(AEEA)$_7$ ("Ligand" in plots) surface loading on AgDNP@Au. Bars show free thiol concentration (extinction at 412 nm) a) after overnight incubation with AgDNP@Au (~0.8 nM). Bound PEX52-Cys-poly(AEEA)$_7$ is calculated as the difference between the ligand-only control and the NP supernatant (orange) in a): 18.05 − 15.87 = 2.18 µM, corresponding to ~2,700 ligands per particle. See "Quantification of CysPoly(AEEA)$_4$ and PEX52-CysPoly(AEEA)$_7$ Surface Coverage by Supernatant Depletion Assay" for full experimental details. b) UV absorbance spectra from the same depletion assay, quantifying PEX52 depletion directly via extinction at 280 nm. The absorbance difference (Δ = 0.012, ε_{280} = 33,535 M^{-1}cm^{-1}) corresponds to a PEX52 depletion of 360 nM, i.e., ~430 proteins per particle and a surface density of 0.14 proteins/nm^2.

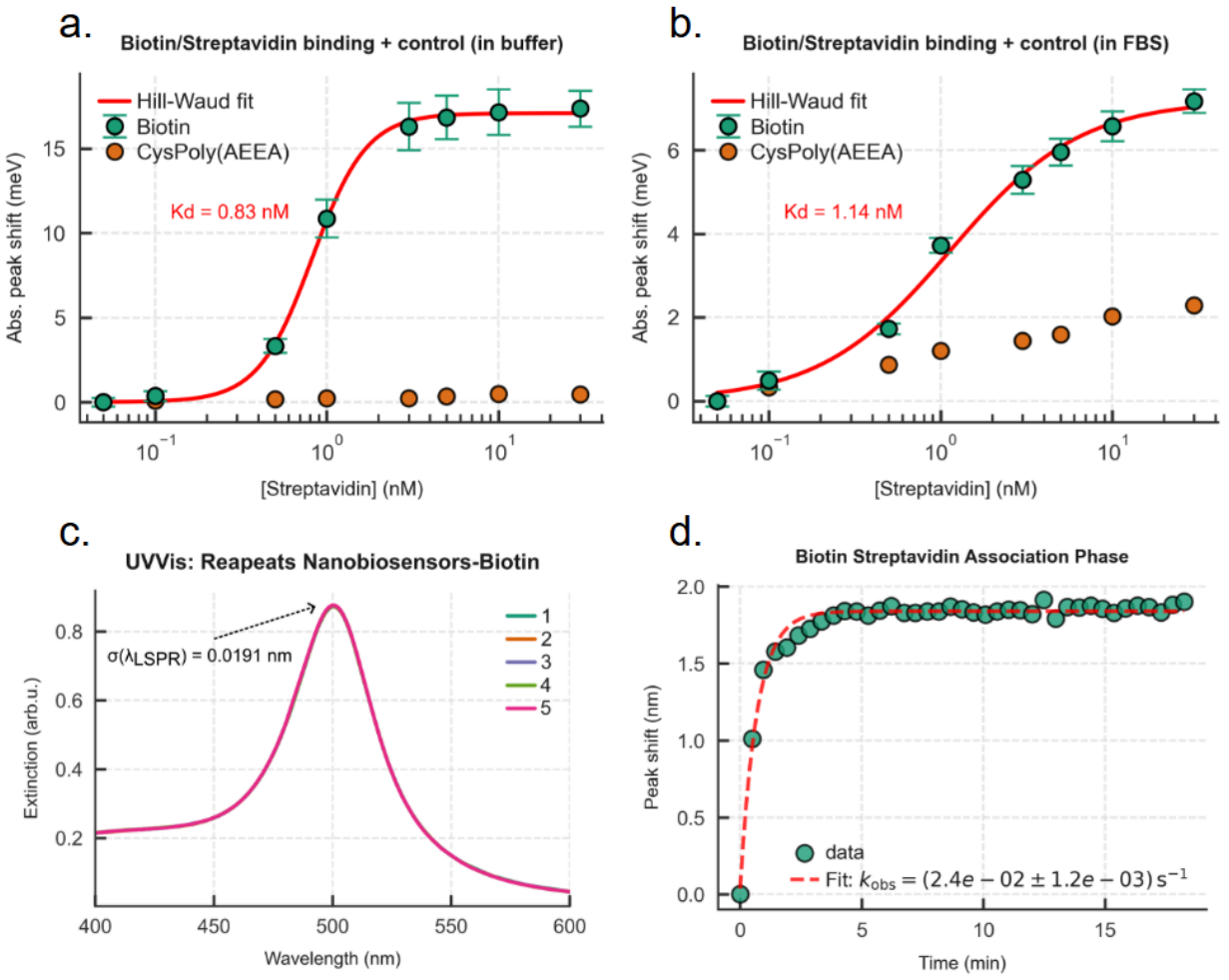


Figure S18: Biotin–streptavidin binding using nanobiosensors modified via SPAAC. Averaged binding titration curves of biotin-conjugated nanobiosensors (SPAAC) during streptavidin titration in (a) buffer and (b) undiluted FBS (teal data), with NPs functionalized with only CysPoly(AEEA) as negative controls (orange). Peak shifts were averaged from three independent binding titration measurements and fitted using the Hill–Waud equation. Teal data points with error bars represent biotinylated nanobiosensors, while orange data points correspond to non-biotinylated controls. (c) UV–vis spectra used to determine the standard deviation of the LSPR peak wavelength, obtained from Gaussian fitting of five consecutive measurements; a deviation of 0.0191 nm was observed.(d) Representative kinetic trace showing streptavidin association under stirring at 800 rpm.

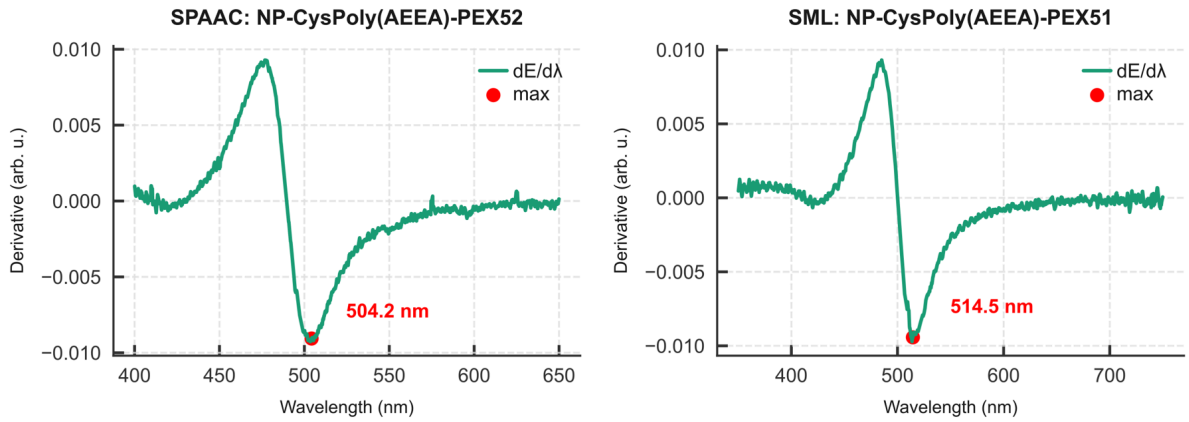


Figure S19: Determination of the optimal single-wavelength readout for kinetic measurements. The point of maximum slope on the red side of the nanoparticle extinction spectrum was identified for nanobiosensors functionalized with PEX52 (SPAAC, left) and PEX51 (SML, right) by recording UV–vis extinction spectra and calculating the minimum of the first derivative (dE/dλ), which defines the steepest spectral region and enables highest-contrast single-wavelength kinetic measurements.

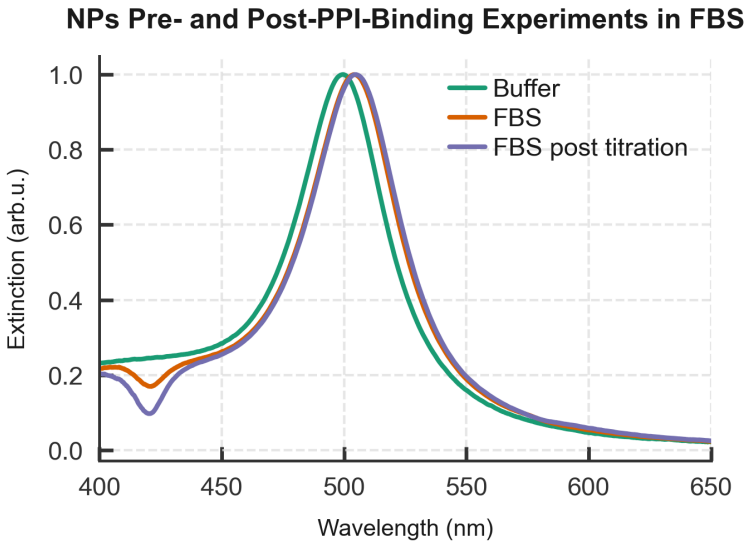


Figure S20: Normalized UV–vis spectra of nanobiosensors before and after a protein-protein interaction binding titration experiment in FBS. The spectra show no signs of aggregation upon introduction of nanoparticles into FBS, as evidenced by the absence of peak broadening or shoulder formation, and remain well-defined after the titration experiment.

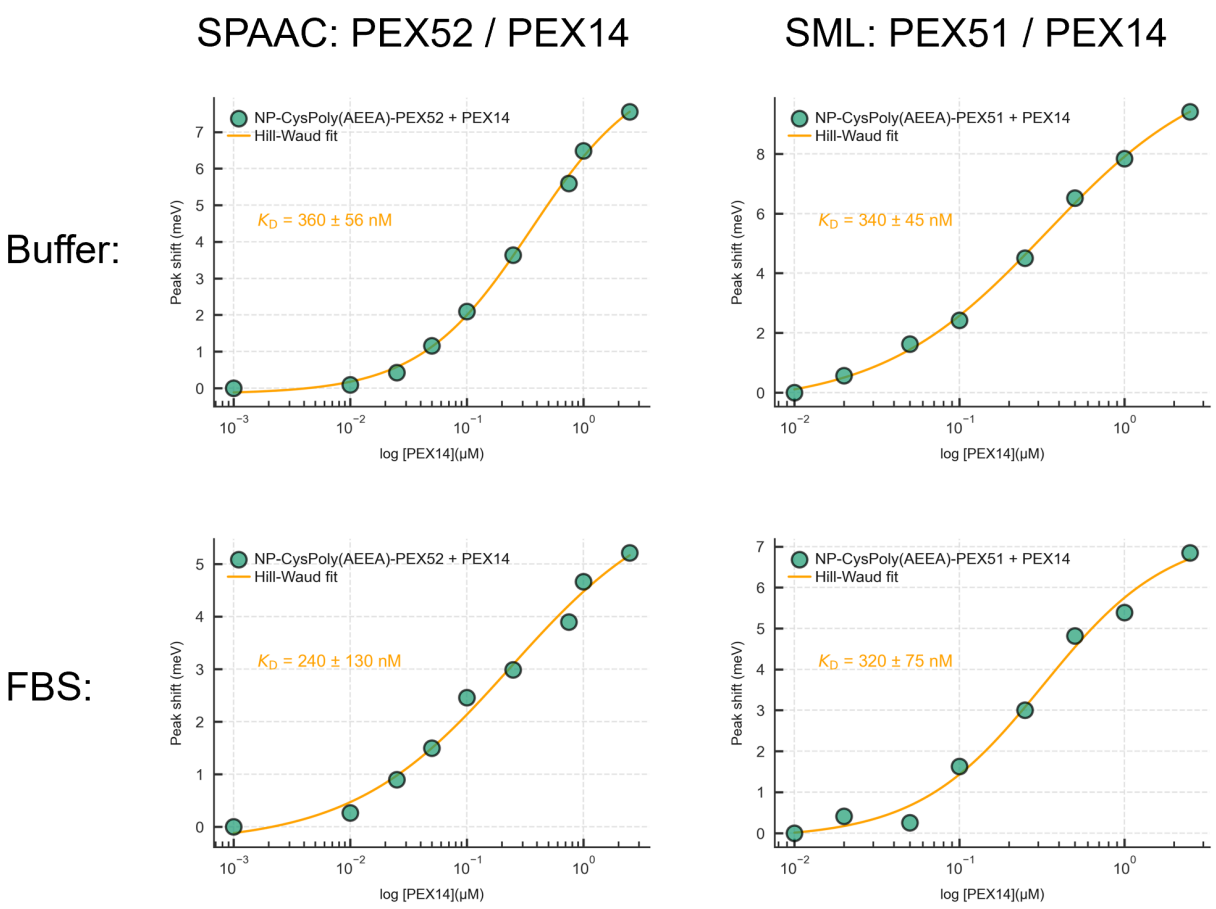


Figure S21: Additional equilibrium binding curves obtained from LSPR peak shifts for PEX5–PEX14 interactions with proteins immobilized via SPAAC (PEX52, left column) or SML (PEX51, right column) in both buffer (upper row) and FBS (bottom row). Note that SPAAC and SML binding experiments were performed by different researchers, on different days and using different NP synthesis batches.

REFERENCES

[1] J. Zhou, K. Ridderbeek, P. Zou, A. B. Naden, S. Gaussmann, F. Song, P. Falter-Braun, E. R. Kay, M. Sattler, J. Cui, *ACS Appl. Opt. Mater.* **2025**, *3*, 676.

[2] S. Gaussmann, M. Gopalswamy, M. Eberhardt, M. Reuter, P. Zou, W. Schliebs, R. Erdmann, M. Sattler, *Front. Cell Dev. Biol.* **2021**, *9*, 651449.

[3] C. Neufeld, F. V. Filipp, B. Simon, A. Neuhaus, N. Schüller, C. David, H. Kooshapur, T. Madl, R. Erdmann, W. Schliebs, M. Wilmanns, M. Sattler, *EMBO J.* **2009**, *28*, 745.

[4] H. M. Beyer, P. Gonschorek, S. L. Samodelov, M. Meier, W. Weber, M. D. Zurbriggen, *PLoS One* **2015**, *10*, e0137652.

[5] L. Freiburger, M. Sonntag, J. Hennig, J. Li, P. Zou, M. Sattler, *J. Biomol. NMR* **2015**, *63*, 1.

[6] M. Gopalswamy, C. Zheng, S. Gaussmann, H. Kooshapur, E. Hambruch, W. Schliebs, R. Erdmann, I. Antes, M. Sattler, *Biol. Chem.* **2023**, *404*, 179.

[7] A. Neuhaus, H. Kooshapur, J. Wolf, N. H. Meyer, T. Madl, J. Saidowsky, E. Hambruch, A. Lazam, M. Jung, M. Sattler, W. Schliebs, R. Erdmann, *J. Biol. Chem.* **2014**, *289*, 437.

[8] J.-Y. Kim, F. Meng, J. Yoo, H. S. Chung, *Nat. Commun.* **2018**, *9*, 4707.

[9] F. Mihalič, E. Åberg, P. Farkhondehkish, N. Theys, E. Andersson, P. Jemth, *Protein Sci.* **2023**, *32*, e4684.

[10] P. Jemth, X. Mu, Å. Engström, J. Dogan, *J. Biol. Chem.* **2014**, *289*, 5528.

[11] Y. K. Choi, N. R. Kern, S. Kim, K. Kanhaiya, Y. Afshar, S. H. Jeon, S. Jo, B. R. Brooks, J. Lee, E. B. Tadmor, H. Heinz, W. Im, *J. Chem. Theory Comput.* **2022**, *18*, 479.

[12] S. Kim, J. Lee, S. Jo, C. L. Brooks 3rd, H. S. Lee, W. Im, *J. Comput. Chem.* **2017**, *38*, 1879.

[13] W. L. Jorgensen, J. Chandrasekhar, J. D. Madura, R. W. Impey, M. L. Klein, *J. Chem. Phys.* **1983**, *79*, 926.

[14] A. Bujacz, *Acta Crystallogr. D Biol. Crystallogr.* **2012**, *68*, 1278.

[15] S. Jo, X. Cheng, S. M. Islam, L. Huang, H. Rui, A. Zhu, H. S. Lee, Y. Qi, W. Han, K. Vanommeslaeghe, A. D. MacKerell Jr, B. Roux, W. Im, *Adv. Protein Chem. Struct. Biol.* **2014**, *96*, 235.

[16] J. Huang, A. D. MacKerell Jr, *J. Comput. Chem.* **2013**, *34*, 2135.

[17] T. Darden, D. York, L. Pedersen, *J. Chem. Phys.* **1993**, *98*, 10089.

[18] B. Hess, H. Bekker, H. J. C. Berendsen, J. G. E. M. Fraaije, *J. Comput. Chem.* **1997**, *18*, 1463.

[19] G. Bussi, D. Donadio, M. Parrinello, *J. Chem. Phys.* **2007**, *126*, 014101.

[20] M. Bernetti, G. Bussi, *J. Chem. Phys.* **2020**, *153*, 114107.

[21] M. Abraham, A. Alekseenko, B. Andrews, V. Basov, P. Bauer, H. Bird, E. Briand, A. Brown, M. Doijade, G. Fiorin, S. Fleischmann, S. Gorelov, G. Gouaillardet, A. Gray, M. E. Irrgang, F. Jalalypour, P. Johansson, C. Kutzner, G. Łazarski, J. A. Lemkul, M. Lundborg, P. Merz, V. Miletić, D. Morozov, L. Müllender, J. Nabet, S. Páll, A. Pasquadibisceglie, M. Pellegrino, N. Piasentin, D. Rapetti, M. U. Sadiq, H. Santuz, R. Schulz, M. Shirts, T. Shugaeva, A. Shvetsov, P. Turner, A. Villa, S. Wingbermühle, B. Hess, E. Lindahl, **2025**

[22] H. Bekker, H. Berendsen, E. J. Dijkstra, S. Achterop, R. Vondrumen, D. Vanderspoel, A. Sijbers, H. Keegstra, M. Renardus, in *PHYSICS COMPUTING '92*, World Scientific Publishing, **1993**, pp. 252–256.

[23] R. Gowers, M. Linke, J. Barnoud, T. Reddy, M. Melo, S. Seyler, J. Domański, D. Dotson, S. Buchoux, I. Kenney, O. Beckstein, in *Proceedings of the Python in Science Conference*, SciPy, **2016**, pp. 98–105.

[24] N. Michaud-Agrawal, E. J. Denning, T. B. Woolf, O. Beckstein, *J. Comput. Chem.* **2011**, *32*,

2319.
[25] E. C. Meng, T. D. Goddard, E. F. Pettersen, G. S. Couch, Z. J. Pearson, J. H. Morris, T. E. Ferrin, *Protein Sci.* **2023**, *32*, e4792.
[26] "Schrödinger, LLC (2015) The PyMOL Molecular Graphics System, Version 1.8. - References - Scientific Research Publishing," can be found under https://www.scirp.org/reference/referencespapers?referenceid=3804901
[27] D. J. Barlow, J. M. Thornton, *J. Mol. Biol.* **1983**, *168*, 867.
[28] E. N. Baker, R. E. Hubbard, *Prog. Biophys. Mol. Biol.* **1984**, *44*, 97.
[29] N. Türkel, *Bioinorganic Chemistry and Applications* **2015**, *2015*, 1.
[30] Z. S. Hendsch, B. Tidor, *Protein Sci.* **1994**, *3*, 211.
[31] C. N. Pace, H. Fu, K. Lee Fryar, J. Landua, S. R. Trevino, D. Schell, R. L. Thurlkill, S. Imura, J. M. Scholtz, K. Gajiwala, J. Sevcik, L. Urbanikova, J. K. Myers, K. Takano, E. J. Hebert, B. A. Shirley, G. R. Grimsley, *Protein Sci.* **2014**, *23*, 652.
[32] J. Wu, S. Chen, *Langmuir* **2012**, *28*, 2137.
[33] E. Hochuli, H. Döbeli, A. Schacher, *J. Chromatogr.* **1987**, *411*, 177.
[34] R. A. Latour, *Colloids Surf. B Biointerfaces* **2020**, *191*, 110992.
[35] G. L. Ellman, *Arch. Biochem. Biophys.* **1958**, *74*, 443.
[36] Y. H. Lee, H. Chen, Q.-H. Xu, J. Wang, *J. Phys. Chem. C* **2011**, *115*, 7997.
[37] K. Rahme, L. Chen, R. G. Hobbs, M. A. Morris, C. O'Driscoll, J. D. Holmes, *RSC Adv.* **2013**, *3*, 6085.
[38] H. Hinterwirth, S. Kappel, T. Waitz, T. Prohaska, W. Lindner, M. Lämmerhofer, *ACS Nano* **2013**, *7*, 1129.
[39] M. Li, S. Jiang, J. Simon, D. Paßlick, M.-L. Frey, M. Wagner, V. Mailänder, D. Crespy, K. Landfester, *Nano Lett.* **2021**, *21*, 1591.
[40] A. Fleming, L. Cursi, J. A. Behan, Y. Yan, Z. Xie, L. Adumeau, K. A. Dawson, *Bioconjug. Chem.* **2022**, *33*, 429.
[41] R. Kozlowski, A. Ragupathi, R. B. Dyer, *Bioconjug. Chem.* **2018**, *29*, 2691.
[42] R. van der Lee, M. Buljan, B. Lang, R. J. Weatheritt, G. W. Daughdrill, A. K. Dunker, M. Fuxreiter, J. Gough, J. Gsponer, D. T. Jones, P. M. Kim, R. W. Kriwacki, C. J. Oldfield, R. V. Pappu, P. Tompa, V. N. Uversky, P. E. Wright, M. M. Babu, *Chem. Rev.* **2014**, *114*, 6589.